Testing the Motion of Strongly Self-Gravitating Bodies with Radio Pulsars

Norbert Wex

Abstract Before the 1970s, precision tests for gravity theories were constrained to the weak-field environment of the Solar System. In terms of relativistic equations of motion, the Solar System gave access to the first order corrections to Newtonian dynamics. Testing anything beyond the first post-Newtonian contributions was for a long time out of reach. The discovery of the first binary pulsar by Russell Hulse and Joseph Taylor in the summer of 1974 initiated a completely new field for testing the relativistic dynamics of gravitationally interacting bodies. For the first time the back reaction of gravitational wave emission on the binary motion could be studied. Furthermore, the Hulse-Taylor pulsar provided the first test bed for the orbital dynamics of strongly self-gravitating bodies. To date, there are a number of binary pulsars known which can be utilized to test different aspects of relativistic dynamics. So far GR has passed these tests with flying colors, while many alternative theories, like scalar-tensor gravity, are tightly constraint by now. This article gives an introduction to gravity tests with pulsars, and summarizes some of the most important results. Furthermore, it gives a brief outlook into the future of this exciting field of experimental gravity.

1 Introduction

In about two years from now we will be celebrating the centenary of Einstein's general theory of relativity. On November 25th 1915 Einstein presented his field equations of gravitation (without cosmological term) to the Prussian Academy of Science [1]. With this publication, general relativity (GR) was finally completed as a logically consistent physical theory (*"Damit ist endlich die allgemeine Relativitätstheorie als logisches Gebäude abgeschlossen."*). Already one week before, based on the vacuum form of his field equations, Einstein was able to show that his theory of gravitation naturally explains the anomalous perihelion advance of the planet

N. Wex (✉)
Max-Planck-Institut für Radioastronomie, Auf dem Hügel 69, 53121 Bonn, Germany
e-mail: wex@mpifr-bonn.mpg.de
URL: http://www.mpifr-bonn.mpg.de/staff/nwex/

D. Puetzfeld et al. (eds.), *Equations of Motion in Relativistic Gravity*,
Fundamental Theories of Physics 179, DOI 10.1007/978-3-319-18335-0_20

Mercury [2]. While in hindsight this can be seen as the first experimental test for GR, back in 1915 astronomers were still searching for a Newtonian explanation [3]. In his 1916 comprehensive summary of GR [4], Einstein proposed three experimental tests:

- Gravitational redshift.
- Light deflection.
- Perihelion precession of planetary orbits.

Gravitational redshift, a consequence of the equivalence principle, is common to all metric theories of gravity, and therefore in some respect its measurement has less discriminating power than the other two tests [5]. The first verification of gravitational light bending during the total eclipse on May 29th 1919 was far from being a high precision test, but clearly decided in favor of GR, against the Newtonian prediction, which is only half the GR value [6]. In the meantime this test has been greatly improved, in the optical with the astrometric satellite HIPPARCOS [7], and in the radio with very long baseline interferometry [8, 9]. The deflection predicted by GR has been verified with a precision of 1.5×10^{-4}. An even better test for the curvature of spacetime in the vicinity of the Sun is based on the Shapiro delay, the so-called "fourth test of GR" [10]. A measurement of the frequency shift of radio signals exchanged with the Cassini spacecraft lead to a 10^{-5} confirmation of GR [11]. Apart from the four "classical" tests, GR has passed many other tests in the Solar system with flying colors: Lunar Laser Ranging tests for the strong equivalence principle and the de-Sitter precession of the Moon's orbit [12], the Gravity Probe B experiment for the relativistic spin precession of a gyroscope (geodetic and frame dragging) [13], and the Lense-Thirring effect in satellite orbits [14], just to name a few.

GR, being a theory where fields travel with finite speed, predicts the existence of gravitational waves that propagate with the speed of light [15] and extract energy from (non-axisymmetric) material systems with accelerated masses [16]. This is also true for a self-gravitating system, where the acceleration of the masses is driven by gravity itself, a question which was settled in a fully satisfactory manner only several decades after Einstein's pioneering papers (see [17] for an excellent review). This fundamental property of GR could not be tested in the slow-motion environment of the Solar system, and the verification of the existence of gravitational waves had to wait until the discovery of the first binary pulsar in 1974 [18]. Also, all the experiments in the Solar system can only test the weak-field aspects of gravity. The spacetime of the Solar system is close to Minkowski space everywhere: To first order (in standard coordinates) the spatial components of the spacetime metric can be written as $g_{ij} = (1 - 2\Phi/c^2)\delta_{ij}$, where Φ denotes the Newtonian gravitational potential. At the surface of the Sun one finds $\Phi/c^2 \sim -2 \times 10^{-6}$, while at the surface of a neutron star $\Phi/c^2 \sim -0.2$. Consequently, gravity experiments with binary pulsars, not only yielded the first tests of the radiative properties of gravity, they also took our gravity tests into a new regime of gravity.

To categorize gravity tests with pulsars and to put them into context with other gravity tests it is useful to introduce the following four gravity regimes:

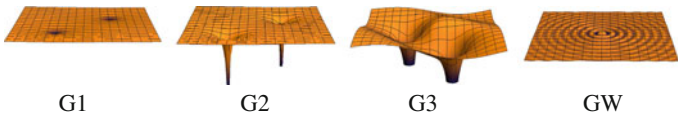

Fig. 1 Illustration of the different gravity regimes used in this article

G1 *Quasi-stationary weak-field regime*: The motion of the masses is slow compared to the speed of light ($v \ll c$) and spacetime is only very weakly curved, i.e. close to Minkowski spacetime everywhere. This is, for instance, the case in the Solar system.

G2 *Quasi-stationary strong-field regime*: The motion of the masses is slow compared to the speed of light ($v \ll c$), but one or more bodies of the system are strongly self-gravitating, i.e. spacetime in their vicinity deviates significantly from Minkowski space. Prime examples here are binary pulsars, consisting of two well-separated neutron stars.

G3 *Highly-dynamical strong-field regime*: Masses move at a significant fraction of the speed of light ($v \sim c$) and spacetime is strongly curved and highly dynamical in the vicinity of the masses. This is the regime of merging neutron stars and black holes.

GW *Radiation regime*: Synonym for the collection of the radiative properties of gravity, most notably the generation of gravitational waves by material sources, the propagation speed of gravitational waves, and their polarization properties.

Figure 1 illustrates the different regimes. Gravity regime G1 is well tested in the Solar system. Binary pulsar experiments are presently our only precision experiments for gravity regime G2, and the best tests for the radiative properties of gravity (regime GW).[1] In the near future, gravitational wave detectors will allow a direct detection of gravitational waves (regime GW) and probe the strong and highly dynamical spacetime of merging compact objects (regime G3). As we will discuss at the end of this article, pulsar timing arrays soon should give us direct access to the nano-Hz gravitational wave band and probe the properties of these ultra-low-frequency gravitational waves (regime GW).

1.1 Radio Pulsars and Pulsar Timing

Radio pulsars, i.e. rotating neutron stars with coherent radio emission along their magnetic poles, were discovered in 1967 by Jocelyn Bell and Antony Hewish [20]. Seven years later, Russell Hulse and Joseph Taylor discovered the first binary pulsar, a pulsar in orbit with a companion star [18]. This discovery marked the beginning of

[1] Gravitational wave damping has also been observed in a double white-dwarf system, which has an orbital period of just 13 min [19]. This experiment combines gravity regimes G1 (note, $v/c \sim 3 \times 10^{-3}$) and GW of Fig. 1.

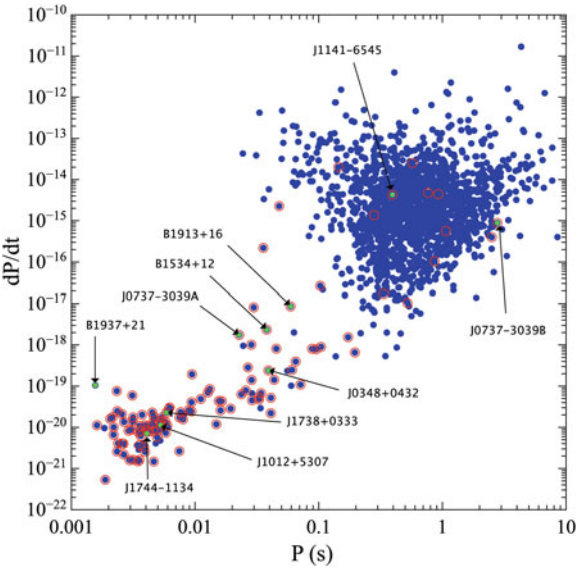

Fig. 2 The P-$\dot{P}$ diagram for radio pulsars. Binary pulsars are indicated by a *red circle*. Pulsars that play a particular role in this article are marked with a *green dot* and have their name as a label. The data are taken from the *ATNF Pulsar Catalogue* [21]

gravity tests with radio pulsars. Presently, more than 2000 radio pulsars are known, out of which about 10 % reside in binary systems [21]. The population of radio pulsars can be nicely presented in a diagram that gives the two main characteristics of a pulsar: the rotational period P and its temporal change $\dot{P}$ due to the loss of rotational energy (see Fig. 2). Fast rotating pulsars with small $\dot{P}$ (millisecond pulsars) appear to be particularly stable in their rotation. On long time-scales, some of them rival the best atomic clocks in terms of stability [22, 23]. This property makes them ideal tools for precision astrometry, and hence (most) gravity tests with pulsars are simply clock comparison experiments to probe the spacetime of the binary pulsar, where the "pulsar clock" is read off by counting the pulses in the pulsar signal (see Fig. 3). As a result, a wide range of relativistic effects related to orbital binary dynamics, time dilation and delays in the signal propagation can be tested. The technique used is the so-called *pulsar timing*, which basically consists of measuring the exact arrival time of pulses at the radio telescope on Earth, and fitting an appropriate *timing model* to these arrival times, to obtain a phase-connected solution. In the phase-connected approach lies the true strength of pulsar timing: the timing model has to account for every (observed) pulse over a time scale of several years, in some cases even several decades. This makes pulsar timing extremely sensitive to even tiny deviations in the model parameters, and therefore vastly superior to a simple measurement of Doppler-shifts in the pulse period. Table 1 illustrates the current precision capabilities of pulsar timing for various experiments, like mass determination, astrometry and gravity tests. We will not go into the details of pulsar observations and pulsar timing here, since there are numerous excellent reviews on these topics, for instance [24, 25], just to mention two. In this article we focus on the relativistic effects that play a role in pulsar-timing observations, and how pulsar timing can be used to test gravitational phenomena in generic as well as theory-based frameworks.

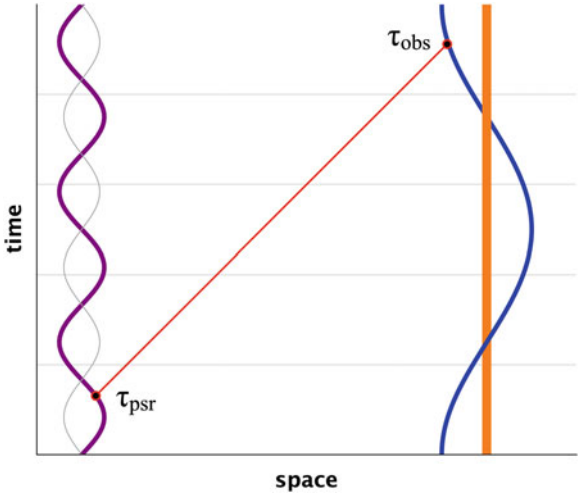

Fig. 3 Spacetime diagram illustration of pulsar timing. Pulsar timing connects the proper time of emission $\tau_{\rm psr}$, defined by the pulsar's intrinsic rotation, and the proper time of the observer on Earth $\tau_{\rm obs}$, measured by the atomic clock at the location of the radio telescope. The timing model, which expresses $\tau_{\rm obs}$ as a function of $\tau_{\rm psr}$, accounts for various "relativistic effects" associated with the metric properties of the spacetime, i.e. the world line of the pulsar and the null-geodesic of the radio signal. In addition, it contains a number of terms related to the Earth motion and relativistic corrections in the Solar system, like time dilation and signal propagation delays (see [26] for details)

Table 1 Examples of precision measurements using pulsar timing

Rotational period	5.757451924362137(2) ms	[27]
Orbital period	0.102251562479(8) d	[*]
Small eccentricity	$(3.5 \pm 1.1) \times 10^{-7}$	[28]
Distance	157(1) pc	[27]
Proper motion	140.915(1) mas yr^{-1}	[27]
Masses of neutron stars	$m_p = 1.4398(2)\ M_\odot$	[29]
	$m_c = 1.3886(2)\ M_\odot$	[29]
Mass of millisecond pulsar	$1.667(7)\ M_\odot$	[30]
Mass of white-dwarf companion	$0.207(2)\ M_\odot$	[31]
Mass of Jupiter and moons	$9.547921(2) \times 10^{-4}\ M_\odot$	[32]
Relativistic periastron advance	4.226598(5) deg yr^{-1}	[29]
Gravitational wave damping	0.504(3) pico-Hz yr^{-1}	[*]
GR validity (observed/GR)	1.0000(5)	[*]

A number in bracket indicates the (one-sigma) uncertainty in the last digit of each value. The symbol $M_\odot$ stands for the Solar mass. (cf. Table 1 in [33])
[*] Kramer et al., in prep.

1.2 Binary Pulsar Motion in Gravity Theories

While in Newtonian gravity there is an exact solution to the equations of motion of two point masses that interact gravitationally, no such exact analytic solution is known in GR. In GR, the two-body problem has to be solved numerically or on the basis of approximation methods. A particularly well established and successful approximation scheme, to tackle the problem of motion of a system of well-separated bodies, is the *post-Newtonian approximation*, which is based on the weak-field slow-motion assumption. However, to describe the motion and gravitational wave emission of binary pulsars, there are two main limitations of the post-Newtonian approximation that have to be overcome (cf. [34]):

(A) Near and inside the pulsar (and its companion, if it is also a neutron star) the gravitational field is strong and the weak-field assumption no longer holds.
(B) When it comes to generation of gravitational waves (of wavelength $\lambda_{\rm GW}$) and their back-reaction on the orbit (of size r and period P_b), the post-Newtonian approximation is only valid in the near zone ($r \ll \lambda_{\rm GW} = cP_b/2$), and breaks down in the radiation zone ($r > \lambda_{\rm GW}$) where gravitational waves propagate and boundary conditions are defined, like the 'no incoming radiation' condition.

The discovery of the Hulse-Taylor pulsar was a particularly strong stimulus for the development of consistent approaches to compute the equations of motion for a binary system with strongly self-gravitating bodies (gravity regime G2). As a result, by now there are fully self-consistent derivations for the gravitational wave emission and the damping of the orbit due to gravitational wave back-reaction for such systems. In fact, in GR, there are several independent approaches that lead to the same result, giving equations of motion for a binary system with non-rotating components that include terms up to 3.5 post-Newtonian order (v^7/c^7) [35, 36]. For the relative acceleration in the center-of-mass frame one finds the general form

$$\ddot{\mathbf{r}} = -\frac{GM}{r^2}\left[(1 + A_2 + A_4 + A_5 + A_6 + A_7)\,\frac{\mathbf{r}}{r} + (B_2 + B_4 + B_5 + B_6 + B_7)\,\dot{\mathbf{r}}\right], \tag{1}$$

where the coefficients A_k and B_k are of order c^{-k}, and are functions of $r \equiv |\mathbf{r}|$, $\dot{r}$, $v \equiv |\dot{\mathbf{r}}|$, and the masses (see [35] for explicit expressions). The quantity M denotes the total mass of the system. At this level of approximation, these equations of motion are also applicable to binaries containing strongly self-gravitating bodies, like neutron stars and black holes. This is a consequence of a remarkable property of Einstein's theory of gravity, the *effacement of the internal structure* [34, 37]: In GR, strong-field contributions are absorbed into the definition of the body's mass.

In GR's post-Newtonian approximation scheme, gravitational wave damping enters for the first time at the 2.5 post-Newtonian level (order v^5/c^5), as a term in the equations of motion that is not invariant against time-reversal. The corresponding loss of orbital energy is given by the *quadrupole formula*, derived for the

first time by Einstein within the linear approximation, for a material system where the gravitational interaction between the masses can be neglected [16]. As it turns out, the quadrupole formula is also applicable for gravity regime G2 of Fig. 1, and therefore valid for binary pulsars as well (cf. [34]).

In alternative gravity theories, the gravitational wave back-reaction, generally, already enters at the 1.5 post-Newtonian level (order v^3/c^3). This is the result of the emission of dipolar gravitational waves, and adds terms A_3 and B_3 to Eq. (1) [5, 38]. Furthermore, one does no longer have an effacement of the internal structure of a compact body, meaning that the orbital dynamics, in addition to the mass, depends on the "sensitivity" of the body, a quantity that depends on its structure/compactness. Such modifications already enter at the "Newtonian" level, where the usual Newtonian gravitational constant G is replaced by a (body-dependent) effective gravitational constant $\mathcal{G}$. For alternative gravity theories, it therefore generally makes an important difference whether the pulsar companion is a compact neutron star or a much less compact white dwarf. In sum, alternative theories of gravity generally predict deviations from GR in both the quasi-stationary and the radiative properties of binary pulsars [39, 40].

At the first post-Newtonian level, for fully conservative gravity theories without preferred location effects, one can construct a generic *modified Einstein-Infeld-Hoffmann Lagrangian* for a system of two gravitationally interacting masses m_p (pulsar) and m_c (companion) at relative (coordinate) separation $r \equiv |\mathbf{x}_p - \mathbf{x}_c|$ and velocities $\mathbf{v}_p = \dot{\mathbf{x}}_p$ and $\mathbf{v}_c = \dot{\mathbf{x}}_c$:

$$\begin{aligned} L_{\rm O} = &-m_p c^2\left(1 - \frac{\mathbf{v}_p^2}{2c^2} - \frac{\mathbf{v}_p^4}{8c^4}\right) - m_c c^2\left(1 - \frac{\mathbf{v}_c^2}{2c^2} - \frac{\mathbf{v}_c^4}{8c^4}\right) \\ &+ \frac{\mathcal{G} m_p m_c}{r}\left[1 - \frac{\mathbf{v}_p\cdot\mathbf{v}_c}{2c^2} - \frac{(\mathbf{r}\cdot\mathbf{v}_p)(\mathbf{r}\cdot\mathbf{v}_c)}{2c^2 r^2} + \varepsilon\frac{(\mathbf{v}_p - \mathbf{v}_c)^2}{2c^2}\right] \\ &- \xi\frac{\mathcal{G}^2 M m_p m_c}{2c^2 r^2}, \end{aligned} \tag{2}$$

where $M \equiv m_p + m_c$. The body-dependent quantities $\mathcal{G}$, ε and ξ account for deviations from GR associated with the self-energy of the individual masses [5, 39]. In GR one simply finds $\mathcal{G} = G$, $\varepsilon = 3$, and $\xi = 1$. There are various analytical solutions to the dynamics of (2). The most widely used in pulsar astronomy is the quasi-Keplerian parametrization by Damour and Deruelle [41]. It forms the basis of pulsar-timing models for relativistic binary pulsars, as we will discuss in more details in Sect. 1.4.

Beyond the first post-Newtonian level there is no fully generic framework for the gravitational dynamics of a binary system. However, one can find equations of motion valid for a general class of gravity theories, like in [42] where a framework based on multi-scalar-tensor theories is introduced to discuss tests of relativistic gravity to the second post-Newtonian level, or in [43] where the explicit equations of motion for non-spinning compact objects to 2.5 post-Newtonian order for a general class of scalar-tensor theories of gravity are given.

1.3 Gravitational Spin Effects in Binary Pulsars

In relativistic gravity theories, in general, the proper rotation of the bodies of a binary system directly affects their orbital and spin dynamics. Equations of motion for spinning bodies in GR have been developed by numerous authors, and in the meantime go way beyond the leading order contributions (for reviews and references see, e.g., [34, 44–46]). For present day pulsar-timing experiments it is sufficient to have a look at the post-Newtonian leading order contributions. There, one finds three contributions: the spin-orbit (SO) interaction between the pulsar's spin $\mathbf{S}_p$ and the orbital angular momentum $\mathbf{L}$, the SO interaction between the companion's spin $\mathbf{S}_c$ and the orbital angular momentum, and finally the spin-spin interaction between the spin of the pulsar and the spin of the companion [44].

Spin-spin interaction will remain negligible in binary pulsar experiments for the foreseeable future. They are many orders of magnitude below the second post-Newtonian and spin-orbit effects [47], and many orders of magnitude below the measurement precision of present timing experiments. For this reason, we will not further discuss spin-spin effects here.

For a boost invariant gravity theory, the (acceleration-dependent) Lagrangian for the spin-orbit interaction has the following general form (summation over spatial indices i, j)

$$L_{\mathrm{SO}}(\mathbf{x}_A, \mathbf{v}_A, \mathbf{a}_A) = \frac{1}{c^2} \sum_A S_A^{ij} \left[\frac{1}{2} v_A^i a_A^j + \sum_{B \neq A} \frac{\Gamma_A^B m_B}{r_{AB}^3} (v_A^i - v_B^i)(x_A^j - x_B^j) \right], \tag{3}$$

where $S_A^{ij} \equiv \varepsilon^{ijk} S_A^k$ is the antisymmetric spin tensor of body A [34, 39, 48]. The coupling function Γ_A^B can also account for strong-field effects in the spin-orbit coupling. In GR $\Gamma_A^B = 2G$. For bodies with negligible gravitational self-energy, one finds in the framework of the *parametrized post-Newtonian (PPN) formalism*[2] $\Gamma_A^B = (\gamma_{\mathrm{PPN}} + 1)G$, a quantity that is actually most tightly constrained by the light-bending and Shapiro-delay experiments in the Solar system, which test γ_{PPN} [8, 9, 11, 49].

In binary pulsars, spin-orbit coupling has two effects. On the one hand, it adds spin-dependent terms to the equations of motion (1), which cause a Lense-Thirring precession of the orbit (for GR see [44, 50]). So far this contribution could not be tested in binary pulsar experiments. Prospects of its measurement will be discussed in the future outlook in Sect. 5. On the other hand it leads to secular changes in the orientation of the spins of the two bodies (geodetic precession), most importantly the observed pulsar in a pulsar binary [44, 51, 52]. As we discuss in more details in Sect. 3, a change in the rotational axis of the pulsar causes changes in the observed

[2] The PPN formalism uses 10 parameters to parametrize in a generic way deviations from GR at the post-Newtonian level, within the class of metric gravity theories (see [5] for details).

emission properties of the pulsar, as the line-of-sight gradually cuts through different regions of the magnetosphere.

As can be derived from (3), to first order in GR the geodetic precession of the pulsar, averaged over one orbit, is given by ($\hat{\mathbf{L}} \equiv \mathbf{L}/|\mathbf{L}|$)

$$\Omega_p^{\rm SO} = \frac{n_b}{1-e^2}\left[2+\frac{3m_c}{2m_p}\right]\frac{m_p m_c}{M^2}\frac{V_b^2}{c^2}\,\hat{\mathbf{L}}, \tag{4}$$

where $n_b \equiv 2\pi/P_b$ and $V_b \equiv (GMn_b)^{1/3}$.

It is expected that in alternative theories relativistic spin precession generally depends on self-gravitational effects, meaning, the actual precession may depend on the compactness of a self-gravitating body. For the class of theories that lead to the Lagrangian (3), Eq. (4) modifies to

$$\Omega_p^{\rm SO} = \frac{n_b}{1-e^2}\left[\frac{\Gamma_p^c}{\mathcal{G}}+\left(\frac{\Gamma_p^c}{\mathcal{G}}-\frac{1}{2}\right)\frac{m_c}{m_p}\right]\frac{m_p m_c}{M^2}\frac{\mathcal{V}_b^2}{c^2}\,\hat{\mathbf{L}}, \tag{5}$$

where $\mathcal{V}_b \equiv (\mathcal{G}Mn_b)^{1/3}$ is the strong-field generalization of V_b.

Effects from spin-induced quadrupole moments are negligible as well. For double neutron-star systems they are many orders of magnitude below the second post-Newtonian and spin-orbit effects, due to the small extension of the bodies [47]. If the companion is a more extended star, like a white dwarf or a main-sequence star, the rotationally-induced quadrupole moment might become important. For all the binary pulsars discussed here, the quadrupole moments of pulsar and companion are (currently) negligible.

Finally, certain gravitational phenomena, not present in GR, can even lead to a spin precession of isolated pulsars, for instance, a violation of the local Lorentz invariance in the gravitational sector, as we will discuss in more details in Sect. 4.

1.4 Phenomenological Approach to Relativistic Effects in Binary Pulsar Observations

For binary pulsar experiments that test the quasi-stationary strong-field regime (G2) and the gravitational wave damping (GW), a phenomenological parametrization, the so-called 'parametrized post-Keplerian' (PPK) formalism, has been introduced by Damour [53] and extended by Damour and Taylor [39]. The PPK formalism parametrizes all the observable effects that can be extracted independently from binary pulsar timing and pulse-structure data. Consequently, the PPK formalism allows to obtain theory-independent information from binary pulsar observations by fitting for a set of *Keplerian* and *post-Keplerian parameters*.

The description of the orbital motion is based on the quasi-Keplerian parametrization of Damour and Deruelle, which is a solution to the first post-Newtonian equations of motion [41, 54]. The corresponding *Roemer delay* in the arrival time of the pulsar signals is

$$\Delta_{\mathrm{R}} = x \sin\omega \left[\cos U - e(1+\delta_r)\right] + x \cos\omega \left[1 - e^2(1+\delta_\theta)^2\right]^{1/2} \sin U, \tag{6}$$

where the eccentric anomaly U is linked to the proper time of the pulsar T via the Kepler equation

$$U - e \sin U = 2\pi \left[\left(\frac{T - T_0}{P_b}\right) - \frac{\dot{P}_b}{2}\left(\frac{T - T_0}{P_b}\right)^2\right]. \tag{7}$$

The five Keplerian parameters P_b, e, x, ω, and T_0 denote the orbital period, the orbital eccentricity, the projected semi-major axis of the pulsar orbit, the longitude of periastron, and the time of periastron passage, respectively. The post-Keplerian parameter δ_r is not separately measurable, i.e. it can be absorbed into other timing parameters, and the post-Keplerian parameter δ_θ has not been measured up to now in any of the binary pulsar systems. The relativistic precession of periastron changes the the longitude of periastron ω according to

$$\omega = \omega_0 + \dot{\omega}\, \frac{P_b}{\pi} \arctan\left[\left(\frac{1+e}{1-e}\right)^{1/2} \tan\frac{U}{2}\right], \tag{8}$$

meaning, that averaged over a full orbit, the location of periastron shifts by an angle $\dot{\omega} P_b$. The parameter $\dot{\omega}$ is the corresponding post-Keplerian parameter. A change in the orbital period, due to the emission of gravitational waves, is parametrized by the post-Keplerian parameter $\dot{P}_b$.

Besides the Roemer delay Δ_{R}, there are two purely relativistic effects that play an important role in pulsar timing experiments. In an eccentric orbit, one has a changing time dilation of the "pulsar clock" due to a variation in the orbital velocity of the pulsar and a change of the gravitational redshift caused by the gravitational field of the companion. This so-called *Einstein delay* is a periodic effect, whose amplitude is given by the post-Keplerian parameter γ, and to first oder can be written as

$$\Delta_{\mathrm{E}} = \gamma \sin U. \tag{9}$$

For sufficiently edge-on and/or eccentric orbits the propagation delay suffered by the pulsar signals in the gravitational field of the companion becomes important. This so-called *Shapiro delay*, to first order, reads

$$\Delta_{\mathrm{S}} = -2r \ln\left[1 - e\cos U - s\sin\omega(\cos U - e) - s\cos\omega(1-e^2)^{1/2}\sin U\right], \tag{10}$$

where the two post-Keplerian parameters r and s are called *range* and *shape* of the Shapiro delay. The latter is linked to the inclination of the orbit with respect to the line of sight, i, by $s = \sin i$. It is important to note, that for $i \to 90°$ Eq. (10) breaks down and higher order corrections are needed. But so far, Eq. (10) is fully sufficient for the timing observations of known pulsars [55].

Concerning the post-Keplerian parameters related to quasi-stationary effects, for the wide class of boost-invariant gravity theories one finds that they can be expressed as functions of the Keplerian parameters, the masses, and parameters generically accounting for gravitational self-field effects (cf. Eq. (2)) [5, 39]:

$$\dot{\omega} = \frac{n_b}{1-e^2}\left[\varepsilon - \frac{\xi}{2} + \frac{1}{2}\right]\frac{\mathcal{V}_b^2}{c^2}, \tag{11}$$

$$\gamma = \frac{e}{n_b}\left[\frac{G_{0c}}{\mathcal{G}} + \mathcal{K}_p^c + \frac{m_c}{M}\right]\frac{m_c}{M}\frac{\mathcal{V}_b^2}{c^2}, \tag{12}$$

$$r = \frac{1+\varepsilon_{0c}}{4}\frac{G_{0c}m_c}{c^3}, \tag{13}$$

$$s = x\, n_b \frac{M}{m_c}\frac{c}{\mathcal{V}_b}, \tag{14}$$

plus Ω^{SO} from Eq. (5). Here we have listed only those parameters that play a role in this article. For a complete list and a more detailed discussion, the reader is referred to [39]. The quantities G_{0c} and ε_{0c} are related to the interaction of the companion with a test particle or a photon. The parameter $\mathcal{K}_p^c$ accounts for a possible change in the moment of inertia of the pulsar due to a change in the local gravitational constant. In GR one finds $\mathcal{G} = G_{0c} = G$, $\varepsilon = \varepsilon_{0c} = 3$, $\xi = 1$ and $\mathcal{K}_p^c = 0$. Consequently

$$\dot{\omega}^{\mathrm{GR}} = \frac{3n_b}{1-e^2}\frac{V_b^2}{c^2}, \tag{15}$$

$$\gamma^{\mathrm{GR}} = \frac{e}{n_b}\left[1 + \frac{m_c}{M}\right]\frac{m_c}{M}\frac{V_b^2}{c^2}, \tag{16}$$

$$r^{\mathrm{GR}} = \frac{Gm_c}{c^3}, \tag{17}$$

$$s^{\mathrm{GR}} = x\, n_b \frac{M}{m_c}\frac{c}{V_b}. \tag{18}$$

These parameters are independent of the internal structure of the neutron star(s), due to the effacement of the internal structure, a property of GR [34, 37]. For most alternative gravity theories this is not the case. For instance, in the mono-scalar-tensor theories $T_1(\alpha_0, \beta_0)$ of [56, 57], one finds[3]

[3]The mono-scalar-tensor theories $T_1(\alpha_0, \beta_0)$ of [56, 57] have a conformal coupling function $A(\varphi) = \alpha_0(\varphi - \varphi_0) + \beta_0(\varphi - \varphi_0)^2/2$. The Jordan-Fierz-Brans-Dicke gravity is the sub-class with $\beta_0 = 0$, and $\alpha_0^2 = (2\omega_{\mathrm{BD}} + 3)^{-1}$.

$$\dot{\omega}^{T_1} = \frac{n_b}{1-e^2}\left[\frac{3-\alpha_p\alpha_c}{1+\alpha_p\alpha_c} - \frac{m_p\alpha_p^2\beta_c + m_c\alpha_c^2\beta_p}{2M(1+\alpha_p\alpha_c)^2}\right]\frac{\mathcal{V}_b^2}{c^2}, \tag{19}$$

$$\gamma^{T_1} = \frac{e}{n_b}\left[\frac{1+k_p\alpha_c}{1+\alpha_p\alpha_c} + \frac{m_c}{M}\right]\frac{m_c}{M}\frac{\mathcal{V}_b^2}{c^2}, \tag{20}$$

$$r^{T_1} = \frac{G_* m_c}{c^3}, \tag{21}$$

$$s^{T_1} = x\, n_b \frac{M}{m_c}\frac{c}{\mathcal{V}_b}, \tag{22}$$

where $\mathcal{V}_b = [G_*(1+\alpha_p\alpha_c)Mn_b]^{1/3}$. The body-dependent quantities α_p and α_c denote the effective scalar coupling of pulsar and companion respectively, and $\beta_A \equiv \partial\alpha_A/\partial\varphi_0$ where φ_0 denotes the asymptotic value of the scalar field at spatial infinity. The quantity k_p is related to the moment of inertia I_p of the pulsar via $k_p \equiv -\partial \ln I_p/\partial\varphi_0$. For a given equation of state, the parameters α_A, β_A, and k_A depend on the fundamental constants of the theory, e.g. α_0 and β_0 in $T_1(\alpha_0, \beta_0)$, and the mass of the body. As we will demonstrate later, these "gravitational form factors" can assume large values in the strong gravitational fields of neutron stars. Depending on the value of β_0, this is even the case for a vanishingly small α_0, where there are practically no measurable deviations from GR in the Solar system. In fact, even for $\alpha_0 = 0$, a neutron star, above a certain β_0-dependent critical mass, can have an effective scalar coupling α_A of order unity. This non-perturbative strong-field behavior, the so-called "spontaneous scalarization" of a neutron star, was discovered 20 years ago by Damour and Esposito-Farèse [56].

Finally, there is the post-Keplerian parameter $\dot{P}_b$, related to the damping of the orbit due to the emission of gravitational waves. We have seen above that in alternative gravity theories the back reaction from the gravitational wave emission might enter the equations of motion already at the 1.5 post-Newtonian level, giving rise to a $\dot{P}_b \propto \mathcal{V}_b^3/c^3$. To leading order one finds in mono-scalar-tensor gravity the dipolar contribution from the scalar field [57–59]:

$$\dot{P}_b = -2\pi \frac{m_p m_c}{M^2}\frac{1+e^2/2}{(1-e^2)^{5/2}}\frac{\mathcal{V}_b^3}{c^3}\frac{(\alpha_p-\alpha_c)^2}{1+\alpha_p\alpha_c} + \mathcal{O}(\mathcal{V}_b^5/c^5). \tag{23}$$

As one can see, the change in the orbital period due to dipolar radiation depends strongly on the difference in the effective scalar coupling α_A. Binary pulsar systems with a high degree of asymmetry in the compactness of their components are therefore ideal to test for dipolar radiation. An order unity difference in the effective scalar coupling would lead to a change in the binary orbit, which is several orders of magnitude ($\sim c^2/\mathcal{V}_b^2$) stronger than the quadrupolar damping predicted by GR. For GR one finds from the well-known *quadrupole formula* [60]:

$$\dot{P}_b^{\mathrm{GR}} = -\frac{192\pi}{5}\frac{m_p m_c}{M^2}\frac{1+73e^2/24+37e^4/96}{(1-e^2)^{7/2}}\frac{V_b^5}{c^5}. \tag{24}$$

Apart from a change in the orbital period, gravitational wave damping will also affect other post-Keplerian parameters. While gravitational waves carry away orbital energy and angular momentum, Keplerian parameters like the eccentricity and the semi-major axis of the pulsar orbit change as well. The corresponding post-Keplerian parameters are $\dot{e}$ and $\dot{x}$ respectively. However, these changes affect the arrival times of the pulsar signals much less than the $\dot{P}_b$, and therefore do (so far) not play a role in the radiative tests with binary pulsars.

As already mentioned in Sect. 1.2, there is no generic connection between the higher-order gravitational wave damping effects and the parameters $\mathcal{G}, \varepsilon$, and ξ of the modified Einstein-Infeld-Hoffmann formalism. Such higher order, mixed radiative and strong-field effects depend in a complicated way on the structure of the gravity theory [39].

The post-Keplerian parameters are at the foundation of many of the gravity tests conducted with binary pulsars. As shown above, the exact functional dependence differs for given theories of gravity. A priori, the masses of the pulsar and the companion are undetermined, but they represent the only unknowns in this set of equations. Hence, once two post-Keplerian parameters are measured, the corresponding equations can be solved for the two masses, and the values for other post-Keplerian parameters can be predicted for an assumed theory of gravity. Any further post-Keplerian measurement must therefore be consistent with that prediction, otherwise the assumed theory has to be rejected. In other words, if $N \geq 3$ post-Keplerian parameters can be measured, a total of $N - 2$ independent tests can be performed. The method is very powerful, as any additionally measured post-Keplerian parameter is potentially able to fail the prediction and hence to falsify the tested theory of gravity. The standard graphical representation of such tests, as will become clear below, is the mass-mass diagram. Every measured post-Keplerian parameter defines a curve of certain width (given by the measurement uncertainty of the post-Keplerian parameter) in a m_p-m_c diagram. A theory has passed a binary pulsar test, if there is a region in the mass-mass diagram that agrees with all post-Keplerian parameter curves.

2 Gravitational Wave Damping

2.1 The Hulse-Taylor Pulsar

The first binary pulsar to ever be observed happened to be a rare double neutron star system. It was discovered by Russell Hulse and Joseph Taylor in summer 1974 [18]. The pulsar, PSR B1913+16, has a rotational period of 59 ms and is in a highly eccentric ($e = 0.62$) 7.75-h orbit around an unseen companion. Shortly after the discovery of PSR B1913+16, it has been realized that this system may allow the observation of gravitational wave damping within a time span of a few years [61, 62].

Table 2 Observed orbital timing parameters of PSR B1913+16, based on the Damour-Deruelle timing model (taken from [29])

T_0	Time of periastron passage (MJD)	52144.90097841(4)
x	Projected semi-major axis of the pulsar orbit (s)	2.341782(3)
e	Orbital eccentricity	0.6171334(5)
P_b	Orbital period at T_0 (d)	0.322997448911(4)
ω_0	Longitude of periastron at T_0 (deg)	292.54472(6)
$\dot{\omega}$	Secular advance of periastron (deg/yr)	4.226598(5)
γ	Amplitude of Einstein delay (ms)	4.2992(8)
$\dot{P}_b$	Secular change of orbital period	$-2.423(1) \times 10^{-12}$

Figures in parentheses represent estimated uncertainties in the last quoted digit

The first relativistic effect seen in the timing observations of the Hulse-Taylor pulsar was the secular advance of periastron $\dot{\omega}$. Thanks to its large value of 4.2 deg/yr, this effect was well measured already one year after the discovery [63]. Due to the, a priori, unknown masses of the system, this measurement could not be converted into a quantitative gravity test. However, assuming GR is correct, Eq. (15) gives the total mass M of the system. From the modern value given in Table 2 one finds $M = m_p + m_c = 2.828378 \pm 0.000007\, M_\odot$ [29].[4]

It took a few more years to measure the Einstein delay (9) with good precision. In a single orbit this effect is exactly degenerate with the Roemer delay, and only due to the relativistic precession of the orbit these two delays become separable [61, 65]. By the end of 1978, the timing of PSR B1913+16 yielded a measurement of the post-Keplerian parameter γ, which is the amplitude of the Einstein delay [66]. Together with the total mass from $\dot{\omega}^{\mathrm{GR}}$, Eq. (16) can now be used to calculate the individual masses. With the modern value for γ from Table 2, and the total mass given above, one finds the individual masses $m_p = 1.4398 \pm 0.0002\, M_\odot$ and $m_c = 1.3886 \pm 0.0002\, M_\odot$ for pulsar and companion respectively [29].

With the knowledge of the two masses, m_p and m_c, the binary system is fully determined, and further GR effects can be calculated and compared with the observed values, providing an intrinsic consistency check of the theory. In fact, Taylor et al. [66] reported the measurement of a decrease in the orbital period $\dot{P}_b$, consistent with the quadrupole formula (24). This was the first proof for the existence of gravitational waves as predicted by GR. In the meantime the $\dot{P}_b$ is measured with a precision of 0.04 % (see Table 2). However, this is not the precision with which the validity of the quadrupole formula is verified in the PSR B1913+16 system. The observed $\dot{P}_b$ needs to be corrected for extrinsic effects, most notably the differential Galactic acceleration and the Shklovskii effect, to obtain the intrinsic value caused by gravitational wave

[4] Strictly speaking, this is the total mass of the system scaled with an unknown Doppler factor D, i.e. $M^{\mathrm{observed}} = D^{-1} M^{\mathrm{intrinsic}}$ [39]. For typical velocities, $D - 1$ is expected to be of order 10^{-4}, see for instance [64]. In gravity tests based on post-Keplerian parameters, the factor D drops out and is therefore irrelevant [54].

damping [67, 68]. The extrinsic contribution due to the Galactic gravitational field (acceleration $\mathbf{g}$) and the proper motion (transverse angular velocity in the sky μ) are given by

$$\delta \dot{P}_b^{\rm ext} = \frac{P_b}{c}\left[\hat{\mathbf{K}}_0 \cdot (\mathbf{g}_{\rm PSR} - \mathbf{g}_\odot) + \mu^2 d\right], \tag{25}$$

where $\hat{\mathbf{K}}_0$ is the unit vector pointing towards the pulsar, which is at a distance d from the Solar system. For PSR B1913+16, P_b and $\hat{\mathbf{K}}_0$ are measured with very high precision, and also μ is known with good precision ($\sim$8 %). However, there is a large uncertainty in the distance d, which is also needed to calculate the Galactic acceleration of the PSR B1913+16 system, $\mathbf{g}_{\rm PSR}$, in Eq. (25). Due to its large distance, there is no direct parallax measurement for d, and estimates of d are based on model-dependent methods, like the measured column density of free electrons between PSR B1913+16 and the Earth. Such methods are known to have large systematic uncertainties, and for this reason the distance to PSR B1913+16 is not well known: $d = 9.9 \pm 3.1$ kpc [29, 69]. In addition, there are further uncertainties, e.g. in the Galactic gravitational potential and the distance of the Earth to the Galactic center. Accounting for all these uncertainties leads to an agreement between $\dot{P}_b - \delta \dot{P}_b^{\rm ext}$ and $\dot{P}_b^{\rm GR}$ at the level of about 0.3 % [29]. The corresponding mass-mass diagram is given in Fig. 4. As the precision of the radiative test with PSR B1913+16 is limited by the model-dependent uncertainties in Eq. (25), it is not expected that this test can be significantly improved in the near future.

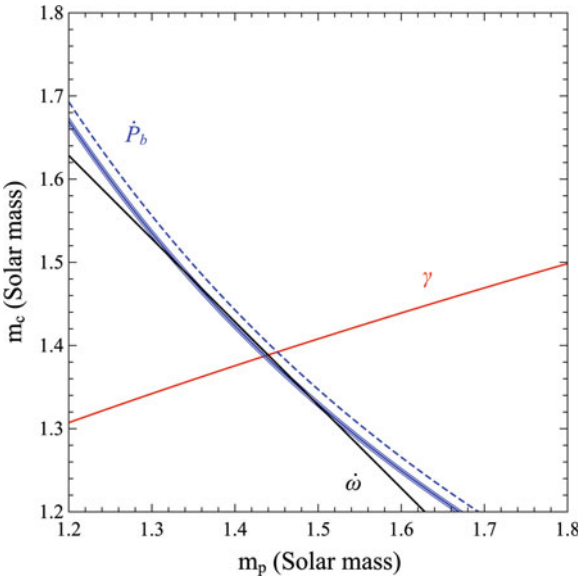

Fig. 4 Mass-mass diagram for PSR B1913+16 based on GR and the three observed post-Keplerian parameters $\dot{\omega}$ (*black*), γ (*red*) and $\dot{P}_b$ (*blue*). The dashed $\dot{P}_b$ curve is based on the observed $\dot{P}_b$, without corrections for Galactic and Shklovskii effects. The solid $\dot{P}_b$ curve is based on the corrected (intrinsic) $\dot{P}_b$, where the *thin lines* indicate the one-sigma boundaries. Values are taken from Table 2

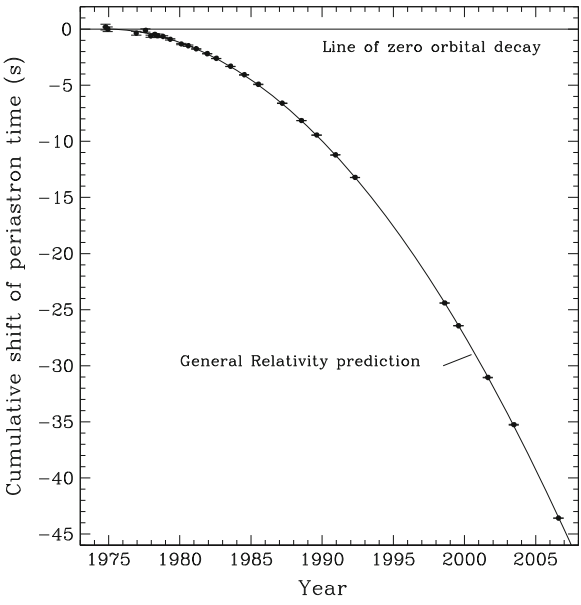

Fig. 5 Shift in the time of periastron passage of PSR B1913+16 due to gravitational wave damping. The parabola represents the GR prediction and the data points the timing measurements, with (*vertical*) *error bars* mostly too small to be resolved. The observed shift in periastron time is a direct measurement of the change in the world-line of the pulsar due to the back-reaction of the emitted gravitational waves (cf. Figure 3). The corresponding spatial shift amounts to about 20,000 km. Figure is taken from [29]

Finally, besides the mass-mass diagram, there is a different way to illustrate the test of gravitational wave damping in PSR B1913+16. According to Eq. (7), the change in the orbital period, i.e. the post-Keplerian parameter $\dot{P}_b$, is measured from a shift in the time of periastron passage, where U is a multiple of 2π. One finds for the shift in periastron time, as compared to an orbit with zero decay

$$\Delta T = \frac{1}{2} P_b \dot{P}_b n^2 + \mathcal{O}(P_b \dot{P}_b^2 n^3), \tag{26}$$

where $n = 0, 1, 2, \ldots$ denotes the number of the periastron passage, and is given by $n \simeq (T - T_0)/P_b$. Equation (26) represents a parabola in time, which can be calculated with high precision using the masses that come from $\dot{\omega}^{\mathrm{GR}}$ and γ^{GR} (see above). On the other hand, the observed cumulative shift in periastron can be extracted from the timing observations with high precision. A comparison of observed and predicted cumulative shift in the time of the periastron passage is given in Fig. 5.

2.2 *The Double Pulsar—The Best Test for Einstein's Quadrupole Formula, and More*

In 2003 a binary system was discovered where, at first, one member was identified as a pulsar with a 23 ms period [70], before about half a year later, the companion was also recognized as a radio pulsar with a period of 2.8 s [71]. Both pulsars, known as

PSRs J0737−3039A and J0737−3039B, respectively, (or A and B hereafter), orbit each other in less than 2.5 h in a mildly eccentric ($e = 0.088$) orbit. As a result, the system is not only the first and only double neutron star system where both neutron stars are visible as active radio pulsars, but it is also the most relativistic binary pulsar laboratory for gravity known to date [72]. Just to give an example for the strength of relativistic effects, the advance of periastron, $\dot{\omega}$, is 17 degrees per year, meaning that the eccentric orbit does a full rotation in just 21 years. In this subsection, we briefly discuss the properties of this unique system, commonly referred to as the *Double Pulsar*, and highlight some of the gravity tests that are based on the radio observations of this system. For detailed reviews of the Double Pulsar see [72, 73].

In the Double Pulsar system a total of six post-Keplerian parameters have been measured by now. Five arise from four different relativistic effects visible in pulsar timing [74], while a sixth one can be determined from the effects of geodetic precession, which will be discussed in detail below. The relativistic precession of the orbit, $\dot{\omega}$, was measured within a few days after timing of the system commenced, and by 2006 it was already known with a precision of 0.004 % (see Table 3). At the same time the measurement of the amplitude of Einstein delay, γ, reached 0.7 % (see Table 3). Due to the periastron precession of 17 degrees per year, the Einstein delay was soon well separable from the Roemer delay. Two further post-Keplerian parameters came from the detection of the Shapiro delay: the *shape* and *range* parameters s and r. They were measured with a precision of 0.04 and 5 %, respectively (see Table 3). From the measured value $s = \sin i = 0.99974^{+0.00016}_{-0.00039}$ ($i = 88.7^{\circ}{}^{+0.5^{\circ}}_{-0.8^{\circ}}$) one can already see how exceptionally edge-on this system is. Finally, the decrease of the orbital period due to gravitational wave damping was measured with a precision of 1.4 % just three years after the discovery of the system (see Table 3).

A unique feature of the Double Pulsar is its nature as a "dual-line source", i.e. we measure the orbits of both neutron stars at the same time. Obviously, the sizes of the two orbits are not independent from each other as they orbit a common center

Table 3 A selection of observed orbital timing parameters of the Double Pulsar, based on the Damour-Deruelle timing model (taken from [74])

$x_A \equiv a_A \sin i/c$	Projected semi-major axis of A (s)	1.415032(1)
$x_B \equiv a_B \sin i/c$	projected semi-major axis of B (s)	1.5161(16)
e	Orbital eccentricity	0.0877775(9)
P_b	Orbital period (d)	0.10225156248(5)
$\dot{\omega}$	Secular advance of periastron (deg/yr)	16.89947(68)
γ	amplitude of Einstein delay for A (ms)	0.3856(26)
$\dot{P}_b$	Secular change of orbital period	$-1.252(17) \times 10^{-12}$
s	*Shape* of Shapiro delay for A	0.99974(−39, +16)
r	*Range* of Shapiro delay for A (μs)	6.21(33)

All post-Keplerian parameters below are obtained from the timing of pulsar A. The timing precision for pulsar B is considerably lower, and allows only for a, in comparison, low precision measurement (∼0.3 %) of $\dot{\omega}$ [74]. Figures in parentheses represent estimated uncertainties in the last quoted digit

of mass. In GR, up to first post-Newtonian order the relative size of the orbits is identical to the inverse ratio of masses. Hence, by measuring the orbits of the two pulsars (relative to the centre of mass), we obtain a precise measurement of the mass ratio. This ratio is directly observable, as the orbital inclination angle is obviously identical for both pulsars, i.e.

$$R \equiv \frac{m_\mathrm{A}}{m_\mathrm{B}} = \frac{a_\mathrm{B}}{a_\mathrm{A}} = \frac{a_\mathrm{B} \sin i/c}{a_\mathrm{A} \sin i/c} \equiv \frac{x_\mathrm{B}}{x_\mathrm{A}}. \tag{27}$$

This expression is not just limited to GR. In fact, it is valid up to first post-Newtonian order and free of any explicit strong-field effects in any Lorentz-invariant theory of gravity (see [40] for a detailed discussion). Using the parameter values of Table 3, one finds that in the Double Pulsar the masses are nearly equal with $R = 1.0714 \pm 0.0011$.

As it turns out, all the post-Keplerian parameters measured from timing are consistent with GR. In addition, the region of allowed masses agrees well with the measured mass ratio R (see Fig. 6). One has to keep in mind, that the test presented here is based on data published in 2006 [74]. In the meantime continued timing lead to a significant decrease in the uncertainties of the post-Keplerian parameters of the Double pulsar. This is especially the case for $\dot{P}_b$, for which the uncertainty typically decreases with $T_\mathrm{obs}^{-2.5}$ [75], T_obs being the total time span of timing observations. The new results will be published in an upcoming publication (Kramer et al., in prep.).

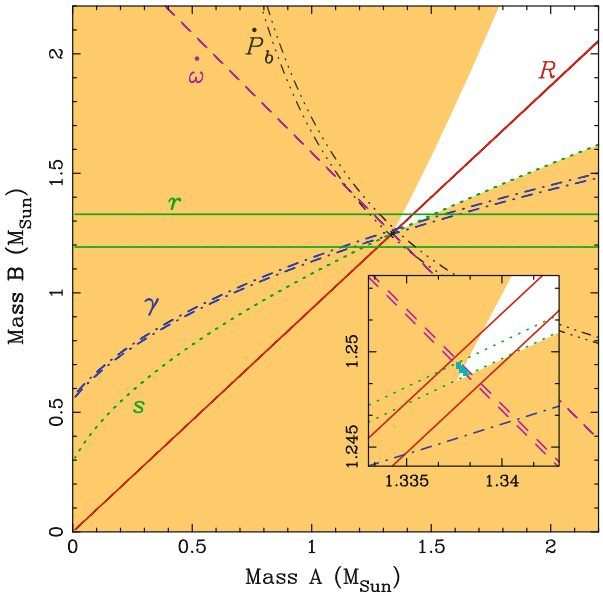

Fig. 6 GR mass-mass diagram based on timing observations of the Double Pulsar. The *orange areas* are excluded simply by the fact that $\sin i \leq 1$. The figure is taken from [72] (Ω_SO lines removed) and based on the timing solution published in [74]

As reported in [33], presently the Double Pulsar provides the best test for the GR quadrupole formalism for gravitational wave generation, with an uncertainty well below the 0.1 % level. As discussed above, the Hulse-Taylor pulsar is presently limited by uncertainties in its distance. This raises the valid question, at which level such uncertainties will start to limit the radiative test with the Double Pulsar as well. Compared to the Hulse-Taylor pulsar, the Double Pulsar is much closer to Earth. Because of this, a direct distance estimate of $1.15^{+0.22}_{-0.16}$ kpc based on a parallax measurement with long-baseline interferometry was obtained [76]. Thus, with the current accuracy in the measurement of distance and transverse velocity, GR tests based on $\dot{P}_b$ can be taken to the 0.01 % level.

With the large number of post-Keplerian parameters and the known mass ratio, the Double Pulsar is the most over-constrained binary pulsar system. For this reason, one can do more than just testing specific gravity theories. The Double Pulsar allows for certain generic tests on the orbital dynamics, time dilation, and photon propagation of a spacetime with two strongly self-gravitating bodies [72]. First, the fact that the Double Pulsar gives access to the mass ratio, R, in any Lorentz-invariant theory of gravity, allows us to determine $m_\mathrm{A}/M = R/(1+R) = 0.51724 \pm 0.00026$ and $m_\mathrm{B}/M = 1/(1+R) = 0.48276 \pm 0.00026$. With this information at hand, the measurement of the shape of the Shapiro delay s can be used to determine $\mathcal{V}_b$ via Eq. (14): $\mathcal{V}_b/c = (2.0854 \pm 0.0014) \times 10^{-3}$. At this point, the measurement of the post-Keplerian parameters $\dot{\omega}$, γ, and r (Eqs. (11)–(13)) can be used to impose restrictions on the "strong-field" parameters of Lagrangian (2) [72]:

$$\frac{2\varepsilon - \xi}{5} = 0.9995 \pm 0.0016, \tag{28}$$

$$\frac{G_{0\mathrm{B}}}{\mathcal{G}} + \mathcal{K}_\mathrm{A}^\mathrm{B} = 1.005 \pm 0.010, \tag{29}$$

$$\frac{\varepsilon_{0\mathrm{B}} + 1}{4}\,\frac{G_{0\mathrm{B}}}{\mathcal{G}} = 1.009 \pm 0.054. \tag{30}$$

This is in full agreement with GR, which predicts one for all three of these expressions. Consequently, nature cannot deviate much from GR in the quasi-stationary strong-field regime of gravity (G2 in Fig. 1).

2.3 PSR J1738+0333—The Best Test for Scalar-Tensor Gravity

The best "pulsar clocks" are found amongst the fully recycled millisecond pulsars, which have rotational periods less than about 10 ms (see e.g. [77]). A result of the stable mass transfer between companion and pulsar in the past—responsible for the recycling of the pulsar—is a very efficient circularization of the binary orbit, that leads to a pulsar-white dwarf system with very small residual eccentricity [78]. For

such systems, the post-Keplerian parameters $\dot{\omega}$ and γ are generally not observable. There are a few cases where the orbit is seen sufficiently edge-on, so that a measurement of the Shapiro delay gives access to the two post-Keplerian parameters r and s with good precision (see e.g. [79], which was the first detection of a Shapiro delay in a binary pulsar). With these two parameters the system is then fully determined, and in principle can be used for a gravity test in combination with a third measured (or constrained) post-Keplerian parameter (e.g. $\dot{P}_b$). Besides the Shapiro delay parameters, some of the circular binary pulsar systems offer a completely different access to their masses, which is not solely based on the timing observations in the radio frequencies. If the companion star is bright enough for optical spectroscopy, then we have a dual-line system, where the Doppler shifts in the spectral lines can be used, together with the timing observations of the pulsar, to determine the mass ratio R. Furthermore, if the companion is a white dwarf, the spectroscopic information in combination with models of the white dwarf and its atmosphere can be used to determine the mass of the white dwarf m_c, ultimately giving the mass of the pulsar via $m_p = R\, m_c$. As we will see in this and the following subsection, two of the best binary pulsar systems for gravity tests have their masses determined through such a combination of radio and optical astronomy.

PSR J1738+0333 was discovered in 2001 [80]. It has a spin period P of 5.85 ms and is a member of a low-eccentricity ($e < 4 \times 10^{-7}$) binary system with an orbital period P_b of just 8.5 h. The companion is an optically bright low-mass white dwarf. Extensive timing observation over a period of 10 years allowed a determination of astrometric, spin and orbital parameters with high precision [28], most notably

- A change in the orbital period of $(-17.0 \pm 3.1) \times 10^{-15}$.
- A timing parallax, which gives a model independent distance estimate of $d = 1.47 \pm 0.10$ kpc.

The latter is important to correct for the Shklovskii effect and the differential Galactic acceleration to obtain the intrinsic $\dot{P}_b$ (cf. Eq. (25)). Additional spectroscopic observations of the white dwarf gave the mass ratio $R = 8.1 \pm 0.2$ and the companion mass $m_c = 0.181^{+0.007}_{-0.005}\, M_\odot$, and consequently the pulsar mass $m_p = 1.47^{+0.07}_{-0.06}\, M_\odot$ [81]. It is important to note, that the mass determination for PSR B1738+0333 is free of any explicit strong-field contributions, since this is the case for the mass ratio [40], and certainly for the mass of the white dwarf, which is a weakly self-gravitating body, i.e. a gravity regime that has been well tested in the Solar system (G1 in Fig. 1).

After using Eq. (25) to correct for the Shklovskii contribution, $\delta \dot{P}_b = P_b \mu^2 d/c = (8.3^{+0.6}_{-0.5}) \times 10^{-15}$, and the contribution from the Galactic differential acceleration, $\delta \dot{P}_b = (0.58^{+0.16}_{-0.14}) \times 10^{-15}$, one finds an intrinsic orbital period change due to gravitational wave damping of $\dot{P}_b^{\rm intr} = (-25.9 \pm 3.2) \times 10^{-15}$. This value agrees well with the prediction of GR, as can be seen in Fig. 7.

The radiative test with PSR J1738+0333 represents a $\sim$15 % verification of GR's quadrupole formula. A comparison with the $<$0.1 % test from the Double Pulsar (see Sect. 2.2) raises the valid question of whether the PSR J1738+0333 experiment is teaching us something new about the nature of gravity and the validity of GR. To

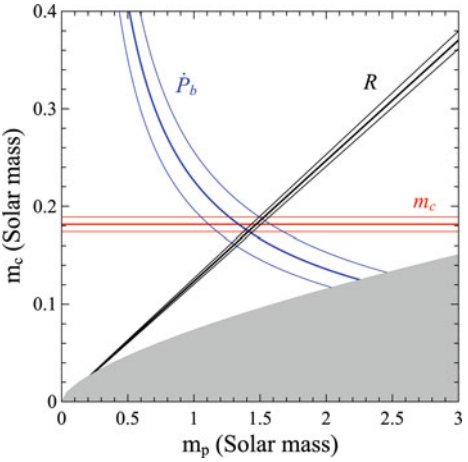

Fig. 7 GR mass-mass diagram based on the timing observations of PSR J1738+0333 and the optical observations of its white-dwarf companion respectively. The *thin lines* indicate the one-sigma errors of the measured parameters. The *grey area* is excluded by the condition $\sin i \leq 1$

address this question, let's have a look at Eq. (23). Dipolar radiation can be a strong source of gravitational wave damping, if there is a sufficient difference between the effective coupling parameters α_p and α_c of pulsar and companion respectively. For the Double Pulsar, where we have two neutron stars with $m_p \approx m_c$, one generally expects that $\alpha_p \approx \alpha_c$, and therefore the effect of dipolar radiation would be strongly suppressed. On the other hand, in the PSR J1738+0333 system there is a large difference in the compactness of the two bodies. For the weakly self-gravitating white-dwarf companion $\alpha_c \simeq \alpha_0$, i.e. it assumes the weak-field value,[5] while the strongly self-gravitating pulsar can have an α_p that significantly deviates from α_0. In fact, as discussed in Sect. 1.4, α_p can even be of oder unity in the presence of effects like strong-field scalarization. In the absence of non-perturbative strong-field effects one can do a first order estimation $(\alpha_p - \alpha_c) \propto (\epsilon_p - \epsilon_c) + \mathcal{O}(\epsilon^2)$. For the Double Pulsar one finds $(\epsilon_p - \epsilon_c)^2 \approx 6 \times 10^{-5}$, which is significantly smaller than for the PSR J1738+0333 system, which has $(\epsilon_p - \epsilon_c)^2 \approx 0.012$.[6] As a consequence, the orbital decay of asymmetric systems like PSR J1738+0333 could still be dominated by dipolar radiation, even if the Double Pulsar agrees with GR. For this reason, PSR J1738+0333 is particularly useful to test gravity theories that violate the strong equivalence principle and therefore predict the emission of dipolar radiation. A well known class of gravity theories, where this is the case, are scalar-tensor theories. As it turns out, PSR J1738+0333 is currently the best test system for these alternatives to GR (see Fig. 8). In terms of Eq. (23), one finds

$$|\alpha_p - \alpha_c| < 2 \times 10^{-3} \quad (95\,\% \text{ confidence}), \tag{31}$$

[5] From the Cassini experiment [11] one obtains $|\alpha_0| < 3 \times 10^{-3}$ (95 % confidence).

[6] These numbers are based on the equation of state MPA1 in [82]. Within GR, MPA1 has a maximum neutron-star mass of 2.46 $M_\odot$, which can also account for the high-mass candidates of [83–85].

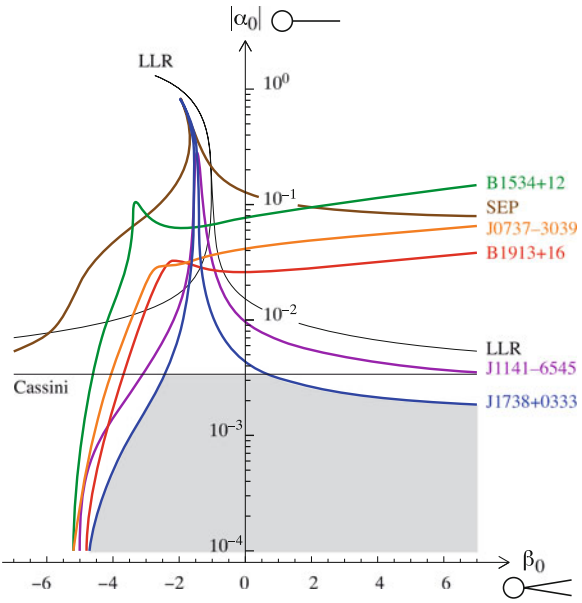

Fig. 8 Constraints on the class of $T_1(\alpha_0, \beta_0)$ scalar-tensor theories of [56, 57], from different binary pulsar and Solar system (Cassini and Lunar Laser Ranging) experiments. The *grey area* indicates the still allowed T_1 theories, and includes GR ($\alpha_0 = \beta_0 = 0$). It is obvious that PSR J1738+0333 is the most constraining experiment for most of the β_0 range, and is even competitive with Cassini in testing the Jordan-Fierz-Brans-Dicke theory ($\beta_0 = 0$). As can be clearly seen, the double neutron-star systems PSR B1534+12 [86], PSR B1913+16 (Hulse-Taylor pulsar) and PSR J0737−3039A/B (Double Pulsar) are considerably less constraining, as explained in the text. Figure is taken from [28]

where for the weakly self-gravitating white dwarf companion $\alpha_c \simeq \alpha_0$. This limit can be interpreted as a generic limit on dipolar radiation, where $\alpha_p - \alpha_c$ is the difference of some hypothetical (scalar- or vector-like) "gravitational charges" [38].

2.4 PSR J0348+0432—A Massive Pulsar in a Relativistic Orbit

PSR J0348+0432 was discovered in 2007 in a drift scan survey using the Green Bank radio telescope (GBT) [87, 88]. PSR J0348+0432 is a mildly recycled radio-pulsar with a spin period of 39 ms. Soon it was found to be in a 2.46-h orbit with a low-mass white-dwarf companion. In fact, the orbital period is only 15 s longer than that of the Double Pulsar, which by itself makes this already an interesting system for gravity. Initial timing observations of the binary yielded an accurate astrometric position, which allowed for an optical identification of its companion [89]. As it turned out, the companion is a relatively bright white dwarf with a spectrum that shows deep Balmer lines. Like in the case of PSR J1738+0333, one could use

high-resolution optical spectroscopy to determine the mass ratio $R = 11.70 \pm 0.13$ and the companion mass $m_c = 0.172 \pm 0.003\, M_\odot$. For the mass of the pulsar one then finds $m_p = R\, m_c = 2.01 \pm 0.04\, M_\odot$, which is presently the highest, well determined neutron star mass, and only the second neutron star with a well determined mass close to $2\, M_\odot$.[7]

Since the discovery of PSR J0348+0432 there have been regular timing observations with three of the major radio telescopes in the world, the 100-m Green Bank Telescope, the 305-m radio telescope at the Arecibo Observatory, and the 100-m Effelsberg radio telescope. Based on the timing data, in 2013 Antoniadis et al. [89] reported the detection of a decrease in the orbital period of $\dot{P}_b = (-2.73 \pm 0.45) \pm 10^{-13}$ that is in full agreement with GR. In numbers:

$$\dot{P}_b / \dot{P}_b^{\mathrm{GR}} = 1.05 \pm 0.18. \tag{32}$$

As it turns out, using the distance inferred from the photometry of the white dwarf ($d \sim 2.1\,\mathrm{kpc}$) corrections due to the Shklovskii effect and differential acceleration in the Galactic potential (see Eq. (25)) are negligible compared to the measurement uncertainty in $\dot{P}_b$.

Like PSR 1738+0333, PSR J0348+0432 is a system with a large asymmetry in the compactness of the components, and therefore well suited for a dipolar radiation test. Using Eq. (23), the limit (32) can be converted into a limit on additional gravitational scalar or vector charges:

$$|\alpha_p - \alpha_0| < 5 \times 10^{-3} \quad (95\,\% \text{ confidence}). \tag{33}$$

This limit is certainly weaker than the limit (32), but it has a new quality as it tests a gravity regime in neutron stars that has not been tested before. Gravity tests before [89] were confined to "canonical" neutron star masses of $\sim 1.4\, M_\odot$. PSR J0348+0432 for the first time allows a test of the relativistic motion of a massive neutron star, which in terms of gravitational self-energy lies clearly outside the tested region (see Fig. 9).

Although an increase in fractional binding energy of about 50 % does not seem much, in the highly non-linear gravity regime of neutron stars it could make a significant difference. To demonstrate this, [89] used the scalar-tensor gravity $T_1(\alpha_0, \beta_0)$ of [56, 57], which is known to behave strongly non-linear in the gravitational fields of neutron stars, in particular for $\beta_0 < -4.0$. As shown in Fig. 10, PSR J0348+0432 excludes a family of scalar-tensor theories that predict significant deviations from GR in massive neutron stars and were not excluded by previous experiments, most notably the test done with PSR J1738+0333.

With PSR J0348+0432, gravity tests now cover a range of neutron star masses from $1.25\, M_\odot$ (PSR J0737−3039B) to $2\, M_\odot$. No significant deviation from GR in the orbital motion of these neutron stars was found. These findings have interesting

[7] The first well determined two Solar mass neutron star is PSR J1614−2230 [90], which is in a wide orbit and therefore does not provide any gravity test.

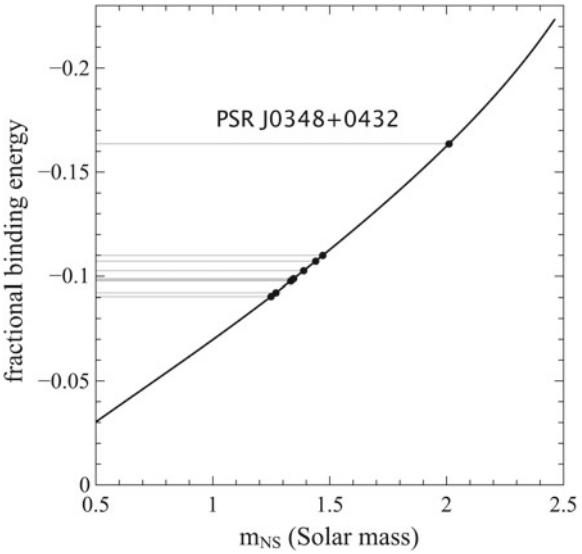

Fig. 9 Fractional gravitational binding energy of a neutron star as a function of its (inertial) mass, based on equation of state MPA1 [82]. The plot clearly shows the prominent position of PSR J0348+0432. The other dots indicate the neutron star masses of the individual test systems in Fig. 8

implications for the upcoming ground-based gravitational wave experiments, as a significant amount of dipolar radiation would drive the phase evolution of the merging binary many cycles away from the GR template and, consequently, degrade the ability to accurately determine the parameters of the merging system or even prevent the detection of the signal. A detailed discussion can be found in [89].

3 Geodetic Precession

A few months after the discovery of the Hulse-Taylor pulsar, Damour and Ruffini [51] proposed a test for geodetic precession in that system. If the pulsar spin is sufficiently tilted with respect to the orbital angular momentum, the spin direction should gradually change over time (see Sect. 1.3). A change in the orientation of the spin-axis of the pulsar with respect to the line-of-sight should lead to changes in the observed pulse profile. These pulse-profile changes manifest themselves in various forms [92], such as changes in the amplitude ratio or separation of pulse components [93, 94], the shape of the characteristic swing of the linear polarization [95], or the absolute value of the position angle of the polarization in the sky [72]. In principle, such changes could allow for a measurement of the precession rate and by this yield a test of GR. In practice, it turned out to be rather difficult to convert changes in the pulse profile into a quantitative test for the precession rate. Indeed, the Hulse-Taylor

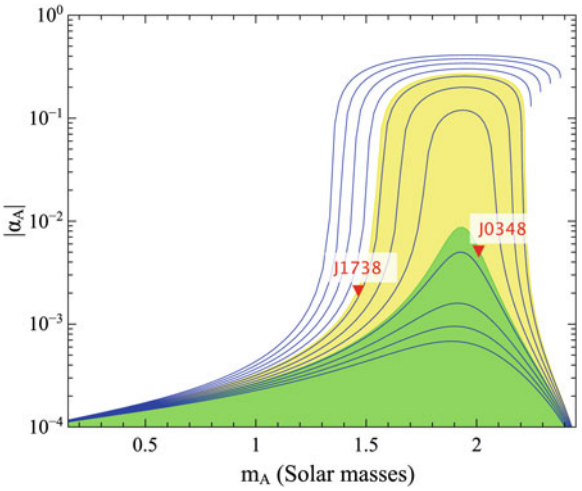

Fig. 10 Effective scalar coupling as a function of the neutron-star mass, in the $T_1(\alpha_0, \beta_0)$ mono-scalar-tensor gravity theory of [56, 57]. For the linear coupling of matter to the scalar field we have chosen $\alpha_0 = 10^{-4}$, a value well below the sensitivity of any near-future Solar system experiment, like GAIA [91]. The *blue curves* correspond to stable neutron-star configurations for different values of the quadratic coupling β_0: -5 to -4 (*top* to *bottom*) in steps of 0.1. The *yellow area* indicates the parameter space still allowed by the limit (31) [label 'J1738'], whereas only the *green area* is in agreement with the limit (33) [label 'J0348']. The plot shows clearly how the massive pulsar PSR J0348+0432 probes deep into a new gravity regime. Neutron-star calculations are based on equation of state MPA1 [82] (see [89] for a different equation-of-state)

pulsar, in spite of prominent profile changes due to geodetic precession [93, 94], does not (yet) allow for a quantitative test of geodetic precession. This is mostly due to uncertainties in the orientation of the magnetic axis and the intrinsic beam shape [96].

Profile and polarization changes due to geodetic precession have been observed in other binary pulsars as well [97, 98], but again did not lead to a quantitative gravity test. A complete list of binary pulsars that up to date show signs of geodetic precession can be found in [33]. Out of the six pulsars listed in [33], so far only two allowed for quantitative constraints on their rate of geodetic precession: PSR B1534+12 [95] and pulsar *B* of the Double Pulsar [99]. In the following we will discuss the latter in more details, as it currently provides the best test for the geodetic precession of a binary pulsar.

In Sect. 2.2, we have seen the Double Pulsar as one of the most exciting "laboratories" for relativistic gravity, with a wealth of relativistic effects measured, allowing the determination of 5 post-Keplerian parameters from timing observations: $\dot{\omega}$, γ, $\dot{P}_b$, r, s. Calculating the inclination angle of the orbit i from $s = \sin i$, one finds that the line-of-sight is inclined with respect to the plane of the binary orbit by just about 1.3° [74]. As a consequence, during the superior conjunction the signals of pulsar *A* pass pulsar *B* at a distance of only 20,000 km. This is small compared to

the extension of pulsar B's magnetosphere, which is roughly given by the radius of the light-cylinder[8] $r_{\rm lc} \equiv cP/2\pi \sim 130{,}000\,\mathrm{km}$. And indeed, at every superior conjunction pulsar A gets eclipsed for about 30 s due to absorption by the plasma in the magnetosphere of pulsar B [71]. A detailed analysis revealed that during every eclipse the light curve of pulsar A shows flux modulations that are spaced by half or integer numbers of pulsar B's rotational period [100]. This pattern can be understood by absorbing plasma that co-rotates with pulsar B and is confined within the closed field lines of the magnetic dipole of pulsar B. As such, the orientation of pulsar B's spin is encoded in the observed light curve of pulsar A [99]. Over the course of several years, Breton et al. [99] observed characteristic shifts in the eclipse pattern, that can be directly related to a precession of the spin of pulsar B. From this analysis, Breton et al. were able to derive a precession rate of

$$\Omega^{\rm SO} = 4.77^{+0.66}_{-0.65}\,\mathrm{deg/yr}. \tag{34}$$

The measured rate of precession is consistent with that predicted by GR ($\Omega^{\rm SO}_{\rm GR} = 5.07\,\mathrm{deg/yr}$) within its one-sigma uncertainty. This is the sixth(!) post-Keplerian parameter measured in the Double-Pulsar system. Furthermore, for the coupling function Γ^A_B, which parametrizes strong-field deviation in alternative gravity theories (see Eq. (5)), one finds

$$\Gamma^A_B/\mathcal{G} = 1.90 \pm 0.22, \tag{35}$$

which agrees with the GR value $\Gamma^A_B/G = 2$. Although the geodetic precession of a gyroscope was confirmed to better than 0.3 % by the Gravity Probe B experiment [13], the clearly less precise test with Double Pulsar B (13 %) for the first time gives a good measurement of this effect for a strongly self-gravitating "gyroscope", and by this represents a qualitatively different test.

The geodetic precession of pulsar B not only changes the pattern of the flux modulations observed during the eclipse of pulsar A, it also changes the orientation of pulsar B's emission beam with respect to our line-of-sight. As a result of this, geodetic precession has by now turned pulsar B in such a way, that since 2009 it is no longer seen by radio telescopes on Earth [101]. From their model, Perera et al. [101] predicted that the reappearance of pulsar A is expected to happen around 2035 with the same part of the beam, but could be as early as 2014 if one assumes a symmetric beam shape.

Finally, for pulsar A GR predicts a precession rate of 4.78 deg/yr, which is comparable to that of pulsar B. However, since the light-cylinder radius of pulsar A ($\sim$1000 km) is considerably smaller than that of pulsar B, there are no eclipses that could give insight into the orientation of its spin. Moreover, long-term pulse profile observations indicate that the misalignment between the spin of pulsar A and the orbital angular momentum is less than 3.2° (95 % confidence) [102]. For such a close alignment, geodetic precession is not expected to cause any significant changes in

[8] The light-cylinder is defined as the surface where the co-rotating frame reaches the speed of light.

the spin direction (cf. Eqs. (4) and (5)). This, on the other hand, is good news for tests based on timing observations. One does not expect a complication in the analysis of the pulse arrival times due to additional modeling of a changing pulse profile.

4 Local Lorentz Invariance of Gravity

Some alternative gravity theories allow the Universal matter distribution to single out the existence of a preferred frame, which breaks the symmetry of local Lorentz invariance (LLI) for the gravitational interaction. In the post-Newtonian parametrization of semi-conservative gravity theories, LLI violation is characterized by two parameters, α_1 and α_2 [5]. Non-vanishing α_1 and α_2 modify the dynamics of self-gravitating systems that move with respect to the preferred frame (preferred-frame effects). In GR one finds $\alpha_1 = \alpha_2 = 0$.

As the most natural preferred frame, generally one chooses the frame associated with the isotropic cosmic microwave background (CMB), meaning that the preferred frame is assumed to be fixed by the global matter distribution of the Universe. From the five-year Wilkinson Microwave Anisotropy Probe (WMAP) satellite experiment, a CMB dipole measurement with high precision was obtained [103]. The CMB dipole corresponds to a motion of the Solar system with respect to the CMB with a velocity of 369.0 ± 0.9 km/s in direction of Galactic longitude and latitude $(l, b) = (263.99^\circ \pm 0.14^\circ, 48.26^\circ \pm 0.03^\circ)$. The numbers quoted in the next two sub-sections, will be with respect to the CMB frame. A generalization to other frames is straightforward, and was done in some of the references cited below.

The most important (weak-field) constraints on preferred-frame effects do come form Lunar Laser Ranging (LLR) [104],

$$\alpha_1 = (-0.7 \pm 1.8) \times 10^{-4} \quad (95\,\%\,\mathrm{CL}), \tag{36}$$

and the alignment of the Sun's spin with the total angular momentum of the planets in the Solar system [105],

$$|\alpha_2| < 2.4 \times 10^{-7}. \tag{37}$$

4.1 Constraints on $\hat{\alpha}_1$ from Binary Pulsars

In binary pulsars, the isotropic violation of Lorentz invariance in the gravitational sector should lead to characteristic preferred frame effects in the binary dynamics, if the barycenter of the binary is moving relative to the preferred frame with a velocity $\mathbf{w}$. For small-eccentricity binaries, the effects induced by $\hat{\alpha}_1$ and $\hat{\alpha}_2$ (the hat indicates possible modifications by strong-field effects) decouple, and can therefore be tested independently [106, 107].

In case of a non-vanishing $\hat{\alpha}_1$, the observed eccentricity vector $\mathbf{e}$ of a small-eccentricity binary pulsar is a vectorial superposition of a 'rotating eccentricity' $\mathbf{e}_R(t)$ and a fixed 'forced eccentricity' $\mathbf{e}_F$: $\mathbf{e}(t) = \mathbf{e}_F + \mathbf{e}_R(t)$ [106]. The rotating eccentricity has a constant length e_R, and rotates with the relativistic precession of periastron, $\dot{\omega}$, in the orbital plane. This is identical to the dynamics caused by a violation of the strong equivalence principle [106, 108], with the forced eccentricity pointing into the direction of $\hat{\mathbf{L}} \times \mathbf{w}$. As a consequence, the binary orbit changes from a less to a more eccentric configuration and back on a time scale of

$$T_{\dot{\omega}} \equiv \frac{2\pi}{\dot{\omega}} \simeq (1140\,\mathrm{yr}) \left(\frac{P_b}{1\,\mathrm{day}}\right)^{5/3} \left(\frac{M}{2M_\odot}\right)^{-2/3}, \tag{38}$$

where we have assumed that the true $\dot{\omega}$ does not deviate significantly from the one predicted by GR (Eq. (15)), an assumption that is well justified by other binary-pulsar experiments, like the generic tests in the Double Pulsar (cf. Sect. 2.2).

The forced eccentricity $\mathbf{e}_F$ is determined by the strength of the preferred frame effect. Its magnitude is approximately given by

$$e_F \simeq 0.093\,\hat{\alpha}_1\,\frac{m_p - m_c}{M} \left(\frac{M}{2M_\odot}\right)^{-1/3} \left(\frac{P_b}{1\,\mathrm{day}}\right)^{1/3} \left(\frac{w\,\sin\psi}{300\,\mathrm{km/s}}\right), \tag{39}$$

where ψ is the angle between $\mathbf{w}$ and $\hat{\mathbf{L}}$ (see [106] for a detailed expression). The observation of small eccentricities in binary pulsars, like $e \sim 10^{-7}$ for PSR J1738+0333 does not directly constrain $\hat{\alpha}_1$. The orientation of the a priory unknown intrinsic $\mathbf{e}_R$ could be such, that it compensates for a large $\mathbf{e}_F$. If the system is sufficiently old, one can assume a uniform probability distribution in $[0°, 360°)$ for $\theta(t)$. Like in the Damour-Schäfer test for SEP, one can now set a probabilistic upper limit on e_F, and by this on $\hat{\alpha}_1$, by excluding θ values close to alignment of $\mathbf{e}_R$ and $\mathbf{e}_F$. Based on this method, [106] found a limit of $|\hat{\alpha}_1| < 5 \times 10^{-4}$ with 90 % confidence.

But even if θ happens to be close to 0°, due to the relativistic precession it will not remain there, and a large e_F cannot remain hidden for ever. In fact, if $\dot{\omega}$ is sufficiently large (greater than ∼1° per year) a significant change in the orbital eccentricity should become observable over time scales of a few years, even if at the start of the observation there was a complete cancellation between $\mathbf{e}_R$ and $\mathbf{e}_F$. This can be used to constrain $\hat{\alpha}_1$ [107]. The best such test comes from PSR J1738+0333 (see Sect. 2.3). This binary pulsar is ideal for this test for several reasons:

- The orbit has an extremely small, well constrained eccentricity of $\sim 10^{-7}$ [28].
- The (calculated) relativistic precession of periastron is about 1.6 deg/yr, and the binary has been observed by now for about 10 years [28]. Hence, $\theta(t)$ has covered an angle of 16° in that time.
- The 3D velocity with respect to the Solar system is known with good precision from timing and optical observations, meaning that one can compute $\mathbf{w}$ [28, 81].

- The orientation of the system is such, that the unknown angle of the ascending node Ω has little influence on the $\hat{\alpha}_1$ limit, hence there is no need for probabilistic considerations to exclude certain values of Ω [107].

Consequently, PSR J1738+0333 leads to the best constraints of α_1-like violations of the local Lorentz invariance of gravity, giving [107]

$$\hat{\alpha}_1 = -0.4^{+3.7}_{-3.1} \times 10^{-5} \quad (95\,\% \text{ confidence}). \tag{40}$$

This limit is not only five times better than the current most stringent limit on α_1 obtained in the Solar system (cf. Eq. (36)), it is also sensitive to potential deviations related to the strong self-gravity of the pulsar. For non-perturbative deviations one can, for illustration purposes, do an expansion with respect to the fractional binding energy ϵ of the neutron star,

$$\hat{\alpha}_1 = \alpha_1 + \mathcal{C}_1\epsilon + \mathcal{O}(\epsilon^2). \tag{41}$$

Since $\epsilon \sim -0.1$ for PSR J1738+0333, we get tight constraints for $\mathcal{C}_1$, a parameter that is virtually unconstraint by the LLR experiment, since $\epsilon \sim -5 \times 10^{-10}$ for the Earth.

4.2 Constraints on $\hat{\alpha}_2$ from Binary and Solitary Pulsars

In the presence of a non-vanishing $\hat{\alpha}_2$, a small-eccentricity binary system experiences a precession of the orbital angular momentum around the fixed direction $\mathbf{w}$ with an angular frequency

$$\Omega^{\text{prec}}_{\hat{\alpha}_2} = -\hat{\alpha}_2 \frac{\pi}{P_b} \left(\frac{w}{c}\right)^2 \cos\psi, \tag{42}$$

where ψ is the angle between the orbital angular momentum and $\mathbf{w}$ [107]. In binary pulsars, such a precession should become visible as a secular change in the projected semi-major axis of the pulsar orbit, $\dot{x}$, which is an observable timing parameter. The two binary pulsars PSRs J1012+5307 and J1738+0333 turn out to be particularly useful for such a test, since both of them have optically bright white dwarf companions, which allowed the determination of the masses in the system, and the 3D systemic velocity with respect to the preferred frame [81, 109, 110].

Unfortunately, in general, the orientation of a binary pulsar orbit with respect to $\mathbf{w}$ and the line-of-sight cannot be fully determined from timing observations. As a consequence, one cannot directly test $\hat{\alpha}_2$ from observed constraints for $\dot{x}$. In fact, since the longitude of the ascending node Ω is not measured, neither for PSR J1012+5307 nor for PSR J1738+0333, the orientation of these systems could in principle be such, that an $\hat{\alpha}_2$-induced precession would not lead to a significant $\dot{x}$. Assuming a random distribution of Ω in the interval $[0°, 360°)$, one can use probabilistic considerations

to exclude such unfavorable orientations. A detailed discussion of this test can be found in [107], where the following 95 % confidence limits are derived

$$\begin{aligned} |\hat{\alpha}_2| &< 3.6 \times 10^{-4} \quad \text{from PSR J1012+5307,} \\ |\hat{\alpha}_2| &< 2.9 \times 10^{-4} \quad \text{from PSR J1738+0333,} \\ |\hat{\alpha}_2| &< 1.8 \times 10^{-4} \quad \text{from PSRs J1012+5307 and J1738+0333 combined.} \end{aligned} \tag{43}$$

It is important to note, that for the last limit, based on the statistical combination of the two systems, one has to assume that $\hat{\alpha}_2$ has only a weak functional dependence on the neutron-star mass in the range of $1.3 - 2.0\, M_\odot$.

The limit for $\hat{\alpha}_2$ obtained from binary pulsars are still several orders of magnitude weaker than the α_2 limit which Nordtvedt derived in 1987 from the alignment of the Sun's spin with the orbital planes of the planets [105]. In the same paper, Nordtvedt pointed out that solitary fast-rotating pulsars could be used in a similar way to obtain tight constraints for α_2. This can be directly seen from Eq. (42), which holds for a rotating self-gravitating star if P_b is replaced by the rotational period P of the star. While the five-billion-year base-line for the Solar experiment is typically a factor of $\sim 10^9$ longer than the observational time-span $T_{\rm obs}$ of pulsars, for millisecond pulsars P is $\sim 10^9$ shorter than the rotational period of the Sun. In fact, the first millisecond pulsar PSR B1937+21, discovered in 1982 [111], by now has a figure of merit $T_{\rm obs}/P$ that is ~ 10 times larger than that of the Sun.

The precession of a solitary pulsar due to a non-vanishing $\hat{\alpha}_2$ would lead to characteristic changes in the observed pulse profile over time-scales of years, just like in the case of binary pulsars that experience geodetic precession (cf. Sect. 3). Consequently, a non-detection of such changes can be converted into constraints for $\hat{\alpha}_2$. Recently, Shao et al. [112] used the two solitary millisecond pulsars PSRs B1937+21 and J1744−1134 for such an experiment. For both pulsars they utilized a consistent set of data, taken over a time span of approximately 15 years with the same observing system at the 100-m Effelsberg radio telescope. The continuity in the observing system was key for an optimal comparison of the high signal-to-noise ratio profiles over time. As it turns out, both pulsars, PSRs B1937+21 and J1744−1134, do not show any detectable profile evolution in the last 15 years. As an example of such a non-detection see Fig. 11, which shows two pulse profiles of PSR B1937+21 obtained at different epochs.

Similarly to the $\hat{\alpha}_2$ test with the binary pulsars, there are unknown angles in the orientation of the pulsar spin, for which certain values have to be excluded based on probabilistic considerations. From extensive Monte-Carlo simulations Shao et al. found with 95 % confidence

$$\begin{aligned} |\hat{\alpha}_2| &< 2.5 \times 10^{-8} \quad \text{from PSR B1937+21,} \\ |\hat{\alpha}_2| &< 1.5 \times 10^{-8} \quad \text{from PSR J1744−1134,} \\ |\hat{\alpha}_2| &< 1.6 \times 10^{-9} \quad \text{from PSRs B1937+21 and J1744−1134 combined.} \end{aligned} \tag{44}$$

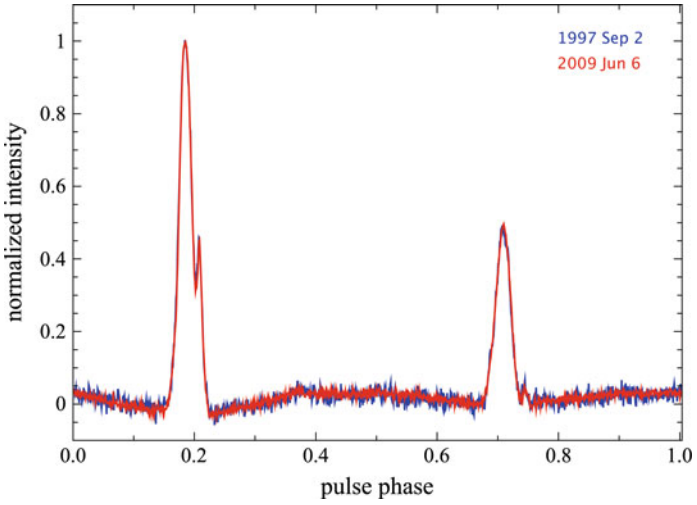

Fig. 11 Comparison of two pulse profiles of PSR B1937+21 obtained at two different epochs. The *blue* one was obtained on September 2, 1997, while the *red* one was obtained on June 6, 2009. The main peak is aligned and scaled to have the same intensity. There exists no visible difference within the noise level. Profiles were taken from [112]

These limits are significantly tighter than the α_2 limit from the Sun's spin orientation. Like in the case of the $\hat{\alpha}_1$ test (previous subsection), this test also covers potential deviations related to the strong self-gravity of the pulsar, and in the combination of the two pulsars, makes the assumption that $\hat{\alpha}_2$ depends only weakly on the neutron-star mass.

An important difference to the aforementioned tests with binary pulsars is, that for solitary pulsars one cannot determine the radial velocity. It enters the determination of $\mathbf{w}$ as a free parameter. However, as shown in [112], the unknown radial velocities for PSRs B1937+21 and J1744−1134 only have a marginal effect on the limits. For the limits above it was assumed that both pulsars are gravitationally bound in the Galactic potential. But even if one relaxes this assumption and allows for unphysically large radial velocities, exceeding 1000 km/s, the limits get weaker by at most ∼40 %.

5 Summary and Outlook

With their discovery of the first binary pulsar four decades ago, Joseph Taylor and Russell Hulse opened a new field of experimental gravity, which has been an active field of research ever since. Besides the Hulse-Taylor pulsar, which led to the first confirmation of the existence of gravitational waves, astronomy has seen the discovery of many new binary pulsars suitable for precision gravity tests. Arguably, the most exiting discovery was the Double Pulsar in 2003, which by now provides the best test for GR's quadrupole formalism of gravitational wave generation (<0.1 % uncertainty),

and the best test for the relativistic spin precession of a strongly self-gravitating body. In addition to this, it is the binary pulsar with the most post-Keplerian parameters measured, allowing for a number of generic constraints on strong-field deviations from GR. For certain aspects of gravity, binary pulsars with white dwarf companions have proven to be even better "test laboratories" than the Double Pulsar. These are gravitational phenomena, predicted by alternatives to GR, that depend on the difference in the compactness/binding energy of the two components, like gravitational dipolar radiation. By now, pulsar-white dwarf systems, like PSR J1738+0333, set quite stringent limits (coupling strength less than about 10^{-3}) on the existence of any additional "gravitational charges" associated with light or massless fields. The recent discovery of a massive pulsar in a relativistic binary system (PSR J0348+0432), for the first time allowed to test the orbital motion of a neutron star that is significantly more compact than pulsars of previous gravity tests. For certain aspects of gravity, solitary pulsars turned out to be ideal probes. The current best limit on the PPN parameters α_2, related to the existence of a preferred frame for gravity, does come from pulse-profile observations of two solitary millisecond pulsars. In all these tests, pulsars go beyond Solar system tests, since they are also sensitive to deviations that occur only in the strong-field environment of neutron stars.

So far, GR has passed all these tests with flying colors. Will this continue for ever? Is GR our final answer to the macroscopic description of gravity? Pulsar astronomy will certainly continue to investigate this question. Many of the tests mentioned here will simply improve by continued timing observations of the known pulsars. In fact, the measurement precision for some of the post-Keplerian parameters increases fast with time. For instance, in regular observations (with the same hardware) the uncertainty in the change of the orbital period $\dot{P}_b$ decreases with $T_{\rm obs}^{-2.5}$, $T_{\rm obs}$ denoting the observing time span. Improvements in the hardware, like new broad-band receivers (e.g. [113]), will further boost the timing precision. For pulsars like PSR J1738+0333 and PSR J0348+0432 soon the modeling of the white dwarf will be the limiting factor, while for the Double Pulsar the corrections of the external contributions to $\dot{P}_b$ will be the challenging bit, in particular if one wants to reach the $\sim 10^{-5}$ level at which higher oder contributions to $\dot{P}_b$ [114, 115] and the Lense-Thirring contribution to the orbital dynamics [44, 50] become relevant (see [72] for a detailed discussion). The upcoming next generation of radio telescopes, like the Five-hundred-meter Aperture Spherical radio Telescope (FAST) [116] and the The Square Kilometre Array (SKA) [117], certainly promise a big step towards this goal. With SKA, for many pulsars one can hope for a factor of 100 improvement in timing precision [118]. The SKA also promises to provide excellent direct distance measurements to pulsars, either directly by utilizing the long baselines of the SKA to form high angular resolution images, or by fitting for the timing parallax in the arrival times of the pulsar signals [119]. In combination with new models for the gravitational potential of our Galaxy, in particular after new missions like GAIA [120], one will be able to accurately determine the extrinsic "contaminations" of $\dot{P}_b$ via Eq. (25), and by this know the intrinsic $\dot{P}_b$. This is key for any high precision gravitational wave test with binary pulsars, but also crucial to measure the Lense-Thirring drag in the Double Pulsar [72].

Reducing the parameter uncertainties for known pulsars is one way to push gravity tests forward, finding new, more relativistic systems is the other. Presently there are a number of pulsar surveys underway that promise the discovery of many new pulsars. New techniques, like acceleration searches [121] and high performance computing, e.g. Einstein@Home [122], promise the detection of pulsars in tight orbits, which generally cannot be found with traditional methods. There is considerable hope among pulsar astronomers, that this will finally also lead to the discovery of a pulsar-black hole system, occasionally called the "holy grail" of pulsar astronomy. Such a system is expected to provide a superb new probe of relativistic gravity and black hole properties, like the dragging of spacetime by the rotation of the black hole [123–125]. According to GR, for an astrophysical black hole (Kerr solution) there is an upper limit for its spin, given by $S_{\max} = GM^2/c$. It would pose an interesting challenge to GR, if the timing of a pulsar-black hole system indicates a spin $S > S_{\max}$. But even for gravity theories that predict the same properties for black holes as in GR, a pulsar-black hole system would constitute an excellent test system, due to the high grade of asymmetry in the strong-field properties of these two components (see [125] for simulations based on $T_1(\alpha_0, \beta_0)$ scalar-tensor theories). A pulsar in a close orbit ($P_b < 1\,\mathrm{yr}$) around the super-massive black hole ($m_{\mathrm{BH}} \approx 4 \times 10^6\, M_\odot$) in the center of our Galaxy would be the ultimate test system, in that context. According to the mock data analysis in [126], for such a system a precise measurement of the quadrupole moment of the black hole, and therefore a test of the no-hair theorem, should be possible, provided that the environment of the pulsar orbit is sufficiently clean. Finding and timing a pulsar in the center of our Galaxy is certainly challenging. A promising result in that direction is the very recent detection of radio signals from a magnetar near the Galactic center black hole [127], even if this pulsar is still too far away from the super-massive black hole ($\sim$0.1 pc) to probe its spacetime.

Until now, all gravitational wave tests are based on probing the near-zone of a binary spacetime by measuring how the back reaction of the gravitational radiation changes the world lines of the source masses. As outlined above, with the Double Pulsar this test has reached a precision of better than 0.1 %. Presently there are considerable efforts to achieve a direct detection of gravitational waves, i.e. measure the far-field properties of such radiative spacetimes by using appropriate test masses. Ground based laser interferometric gravitational wave observatories, like LIGO and VIRGO, have mirrors with separations of a few kilometers. Their sensitivity is in the range from 10 Hz to few 10^3 Hz. Planned space-based detectors, like eLISA, will have three drag-free satellites as test masses with a typical separation of $\sim 10^6$ km, and should be sensitive to gravitational waves from about 10^{-4} to 0.1 Hz. For the ultra-low frequency band (few nano-Hz) pulsar timing arrays are currently the most promising detectors [128]. In these experiments the Earth/Solar system and a collection of very stable pulsars act as the test masses. A gravitational wave becomes apparent in a pulsar timing array by the changes it causes in the arrival times of the pulsar signals. Due to the fitting of the rotational frequency ν and its time derivative $\dot{\nu}$ for every pulsar, such

a detector is only sensitive to wavelengths up to $\sim c\, T_{\rm obs}$.[9] This leads to the special situation that the length of the "detector arms" is much larger than the wavelength. As a consequence, the observed timing signal contains two contributions, the so-called *pulsar term*, related to the impact of the gravitational wave on the pulsar when the radio signal is emitted, and the *Earth term* corresponding to the impact of the gravitational wave on the Earth during the arrival of the radio signal at the telescope [131, 132]. The most promising source in the nano-Hz frequency band is a stochastic gravitational wave background, as a result of many mergers of super-massive black hole binaries in the past history of the Universe [133, 134]. With the large number of "detector arms", pulsar timing arrays have enough information to explore the properties of the nano-Hz gravitational wave background in details, once its signal is clearly detected in the data. Are there more than the two Einsteinian polarization modes (alternative metric theories can have up to six)? Is the propagation speed of nano-Hz gravitational waves frequency depended? Does the graviton carry mass? These are some of the main questions that can be addressed with pulsar timing arrays [135, 136]. The isolation of a single source in the pulsar timing array data would give us a unique opportunity to study the merger evolution of a super-massive black hole binary, since the signal in the Earth term and the signal in the pulsar term show two different states of the system, which are typically several thousand years apart [137]. For these kind of gravity experiments, however, we might have to wait till the full SKA has collected a few years of data, which probably brings us close to the year 2030.

Acknowledgments I would like to thank the workshop organizers for their hospitality, and John Antoniadis for carefully reading the manuscript.

References

1. A. Einstein, Sitzungsberichte der Königlich Preußischen Akademie der Wissenschaften (Berlin), pp. 844–847 (1915)
2. A. Einstein, Sitzungsberichte der Königlich Preußischen Akademie der Wissenschaften (Berlin), pp. 831–839 (1915)
3. H. Seeliger, Astronomische Nachrichten **201**, 273 (1915)
4. A. Einstein, Annalen der Physik **354**, 769–822 (1916)
5. C.M. Will, *Theory and Experiment in Gravitational Physics,* 2nd edn. (Cambridge University Press, Cambridge, 1993)
6. F.W. Dyson, A.S. Eddington, C. Davidson, R. Soc. Lond. Philos. Trans. Ser. A **220**, 291–333 (1920)
7. M. Froeschle, F. Mignard, F. Arenou, in *Hipparcos—Venice'97*, vol. 402, ed. by R.M. Bonnet, E. Høg, P.L. Bernacca, et al. (ESA Special Publication, The Netherlands, 1997), pp. 49–52
8. S.S. Shapiro, J.L. Davis, D.E. Lebach, J.S. Gregory, Phys. Rev. Lett. **92**, 121101 (2004)
9. E. Fomalont, S. Kopeikin, G. Lanyi, J. Benson, Astrophys. J. **699**, 1395–1402 (2009)
10. I.I. Shapiro, Phys. Rev. Lett. **13**, 789–791 (1964)

[9] It has been suggested to use the orbital period of binary pulsars to test for gravitational waves of considerably longer wavelength [129, 130].

11. B. Bertotti, L. Iess, P. Tortora, Nature **425**, 374–376 (2003)
12. K. Nordtvedt, Class. Quantum Gravity **16**, A101–A112 (1999)
13. C.W.F. Everitt, D.B. Debra, B.W. Parkinson et al., Phys. Rev. Lett. **106**, 221101 (2011)
14. I. Ciufolini, E.C. Pavlis, Nature **431**, 958–960 (2004)
15. A. Einstein, Sitzungsberichte der Königlich Preußischen Akademie der Wissenschaften (Berlin), pp. 688–696 (1916)
16. A. Einstein, Sitzungsberichte der Königlich Preußischen Akademie der Wissenschaften (Berlin), pp. 154–167 (1918)
17. D. Kennefick, *Traveling at the Speed of Thought: Einstein and the Quest for Gravitational Waves,* (Princeton University Press, Princeton, 2007)
18. R.A. Hulse, J.H. Taylor, Astrophys. J. **195**, L51–L53 (1975)
19. J.J. Hermes, M. Kilic, W.R. Brown et al., Astrophys. J. **757**, L21 (2012)
20. A. Hewish, S.J. Bell, J.D.H. Pilkington et al., Nature **217**, 709–713 (1968)
21. R.N. Manchester, G.B. Hobbs, A. Teoh, M. Hobbs, Astrophys. J. **129**, 1993–2006 (2005). http://www.atnf.csiro.au/research/pulsar/psrcat/
22. D.R. Lorimer, Living Rev. Relativ, **8** (2005). http://www.livingreviews.org/lrr-2005-7
23. G. Hobbs, W. Coles, R.N. Manchester et al., Mon. Not. R. Astron. Soc. **427**, 2780–2787 (2012)
24. I.H. Stairs, Living Rev. Relativ. **6** (2003). http://www.livingreviews.org/lrr-2003-5
25. D.R. Lorimer, M. Kramer, *Handbook of Pulsar Astronomy,* (Cambridge University Press, Cambridge, 2004)
26. R.T. Edwards, G.B. Hobbs, R.N. Manchester, Mon. Not. R. Astron. Soc. **372**, 1549–1574 (2006)
27. J.P.W. Verbiest, M. Bailes, W. van Straten et al., Astrophys. J. **679**, 675–680 (2008)
28. P.C.C. Freire, N. Wex, G. Esposito-Farèse et al., Mon. Not. R. Astron. Soc. **423**, 3328–3343 (2012)
29. J.M. Weisberg, D.J. Nice, J.H. Taylor, Astrophys. J. **722**, 1030–1034 (2010)
30. P.C.C. Freire, C.G. Bassa, N. Wex et al., Mon. Not. R. Astron. Soc. **412**, 2763–2780 (2011)
31. A.W. Hotan, M. Bailes, S.M. Ord, Mon. Not. R. Astron. Soc. **369**, 1502–1520 (2006)
32. D.J. Champion, G.B. Hobbs, R.N. Manchester et al., Astrophys. J. **720**, L201–L205 (2010)
33. M. Kramer, Proc. Int. Astron. Union **8**, 19–26 (2012)
34. T. Damour, in *Three Hundred Years of Gravitation*, ed. by S.W. Hawking, W. Israel (Cambridge University Press, Cambridge, 1987), pp. 128–198
35. L. Blanchet, Living Rev. Relativ. **9**, 4 (2006)
36. T. Futamase, Y. Itoh, Living Rev. Relativ. **10** (2007). http://www.livingreviews.org/lrr-2007-2
37. T. Damour, in *Gravitational Radiation*, ed. by N. Deruelle, T. Piran (North-Holland, Amsterdam, 1983), pp. 59–144
38. J.-M. Gérard, Y. Wiaux, Phys. Rev. D **66**, 024040 (2002)
39. T. Damour, J.H. Taylor, Phys. Rev. D **45**, 1840–1868 (1992)
40. T. Damour, in *Astrophysics and Space Science Library*, vol. 359, ed. by M. Colpi, P. Casella, V. Gorini, U. Moschella, A. Possenti (Springer, New York, 2009), pp. 1–41
41. T. Damour, N. Deruelle, Ann. Inst. Henri Poincaré Phys. Théor. **43**, 107–132 (1985)
42. T. Damour, G. Esposito-Farèse, Phys. Rev. D **53**, 5541–5578 (1996)
43. S. Mirshekari, C.M. Will, Phys. Rev. D **87**, 084070 (2013)
44. B.M. Barker, R.F. O'Connell, Phys. Rev. D **12**, 329–335 (1975)
45. V.A. Brumberg, *Essential Relativistic Celestial Mechanics,* (Adam Hilger, Bristol, 1991)
46. J. Hartung, J. Steinhoff, G. Schäfer, Annalen der Physik **525**, 359–394 (2013)
47. N. Wex, Class. Quantum Gravity **12**, 983–1005 (1995)
48. T. Damour, C. R. Acad. Sci. Paris Sér. II **294**, 1355–1357 (1982)
49. D.E. Lebach, B.E. Corey, I.I. Shapiro et al., Phys. Rev. Lett. **75**, 1439–1442 (1995)
50. T. Damour, G. Schäfer, Nuovo Cimento B **101**, 127 (1988)
51. T. Damour, R. Ruffini, Academie des Sciences Paris Comptes Rendus Serie Sciences Mathematiques **279**, 971–973 (1974)

52. G. Börner, J. Ehlers, E. Rudolph, Astron. Astrophys. **44**, 417–420 (1975)
53. T. Damour, in *Proceedings of the 2nd Canadian Conference on General Relativity and Relativistic Astrophysics*, ed. by A. Coley, C. Dyer, T. Tupper, (University of Toronto, 1988), pp. 315–334
54. T. Damour, N. Deruelle, Ann. Inst. Henri Poincaré Phys. Théor. **44**, 263–292 (1986)
55. M. Ali, Master thesis, University of Bonn, Germany (2011)
56. T. Damour, G. Esposito-Farèse, Phys. Rev. Lett. **70**, 2220–2223 (1993)
57. T. Damour, G. Esposito-Farèse, Phys. Rev. D **54**, 1474–1491 (1996)
58. D.M. Eardley, Astrophys. J. **196**, L59–L62 (1975)
59. C.M. Will, Astrophys. J. **214**, 826–839 (1977)
60. P.C. Peters, Phys. Rev. **136**, B1224–B1232 (1964)
61. V.A. Brumberg, I.B. Zeldovich, I.D. Novikov, N.I. Shakura, Sov. Astron. Lett. **1**, 2–4 (1975)
62. R.V. Wagoner, Astrophys. J. **196**, L63–L65 (1975)
63. J.H. Taylor, R.A. Hulse, L.A. Fowler et al., Astrophys. J. **206**, L53–L58 (1976)
64. N. Wex, V. Kalogera, M. Kramer, Astrophys. J. **528**, 401–409 (2000)
65. R. Blandford, S.A. Teukolsky, Astrophys. J. **198**, L27–L29 (1975)
66. J.H. Taylor, L.A. Fowler, P.M. McCulloch, Nature **277**, 437–440 (1979)
67. I.S. Shklovskii, Sov. Astron. **13**, 562–565 (1970)
68. T. Damour, J.H. Taylor, Astrophys. J. **366**, 501–511 (1991)
69. J.M. Weisberg, S. Stanimirović, K. Xilouris et al., Astrophys. J. **674**, 286–294 (2008)
70. M. Burgay, N. D'Amico, A. Possenti et al., Nature **426**, 531–533 (2003)
71. A.G. Lyne, M. Burgay, M. Kramer et al., Science **303**, 1153–1157 (2004)
72. M. Kramer, N. Wex, Class. Quantum Gravity **26**, 073001 (2009)
73. M. Kramer, I.H. Stairs, Annu. Rev. Astron. Astrophys. **46**, 541–572 (2008)
74. M. Kramer, I.H. Stairs, R.N. Manchester et al., Science **314**, 97–102 (2006)
75. R. Blandford, S.A. Teukolsky, Astrophys. J. **205**, 580–591 (1976)
76. A.T. Deller, M. Bailes, S.J. Tingay, Science **323**, 1327–1329 (2009)
77. J.P.W. Verbiest, M. Bailes, W.A. Coles et al., Mon. Not. R. Astron. Soc. **400**, 951–968 (2009)
78. E.S. Phinney, R. Soc. Lond. Philos. Trans. Ser. A **341**, 39–75 (1992)
79. M.F. Ryba, J.H. Taylor, Astrophys. J. **371**, 739–748 (1991)
80. B.A. Jacoby, Ph.D. thesis, California Institute of Technology, California, USA (2005)
81. J. Antoniadis, M.H. van Kerkwijk, D. Koester et al., Mon. Not. R. Astron. Soc. **423**, 3316–3327 (2012)
82. H. Müther, M. Prakash, T.L. Ainsworth, Phys. Lett. B **199**, 469–474 (1987)
83. P.C.C. Freire, S.M. Ransom, S. Bégin et al., Astrophys. J. **675**, 670–682 (2008)
84. M.H. van Kerkwijk, R.P. Breton, S.R. Kulkarni, Astrophys. J. **728**, 95 (2011)
85. R.W. Romani, A.V. Filippenko, J.M. Silverman et al., Astrophys. J. **760**, L36 (2012)
86. I.H. Stairs, S.E. Thorsett, J.H. Taylor, A. Wolszczan, Astrophys. J. **581**, 501–508 (2002)
87. J. Boyles, R.S. Lynch, S.M. Ransom et al., Astrophys. J. **763**, 80 (2013)
88. R.S. Lynch, J. Boyles, S.M. Ransom et al., Astrophys. J. **763**, 81 (2013)
89. J. Antoniadis, P.C.C. Freire, N. Wex et al., Science **340**, 448 (2013)
90. P.B. Demorest, T. Pennucci, S.M. Ransom et al., Nature **467**, 1081–1083 (2010)
91. D. Hobbs, B. Holl, L. Lindegren et al., Proc. Int. Astron. Union **5**, 315–319 (2009)
92. N.D.H. Dass, V. Radhakrishnan, Astrophys. J. **16**, L135–L139 (1975)
93. J.M. Weisberg, R.W. Romani, J.H. Taylor, Astrophys. J. **347**, 1030–1033 (1989)
94. M. Kramer, Astrophys. J. **509**, 856–860 (1998)
95. I.H. Stairs, S.E. Thorsett, Z. Arzoumanian, Phys. Rev. Lett. **93**, 141101 (2004)
96. J.M. Weisberg, J.H. Taylor, Astrophys. J. **576**, 942–949 (2002)
97. R.N. Manchester, M. Kramer, I.H. Stairs et al., Astrophys. J. **710**, 1694–1709 (2010)
98. G. Desvignes, M. Kramer, I. Cognard et al., Proc. Int. Astron. Union **8**, 199–202 (2012)
99. R.P. Breton, V.M. Kaspi, M. Kramer et al., Science **321**, 104–107 (2008)
100. M.A. McLaughlin, A.G. Lyne, D.R. Lorimer et al., Astrophys. J. **616**, L131–L134 (2004)
101. B.B.P. Perera, M.A. McLaughlin, M. Kramer et al., Astrophys. J. **721**, 1193–1205 (2010)
102. R.D. Ferdman, I.H. Stairs, M. Kramer et al., Astrophys. J. **767**, 85 (2013)

103. G. Hinshaw, J.L. Weiland, R.S. Hill et al., Astrophys. J. Suppl. **180**, 225–245 (2009)
104. J. Müller, J.G. Williams, S.G. Turyshev, Astrophysics and space science library, in *Lasers, Clocks and Drag-Free Control: Exploration of Relativistic Gravity in Space*, vol. 349, ed. by H. Dittus, C. Lammerzahl, S.G. Turyshev (Springer, Berlin, 2008), pp. 457–472
105. K. Nordtvedt, Astrophys. J. **320**, 871–874 (1987)
106. T. Damour, G. Esposito-Farèse, Phys. Rev. D **46**, 4128–4132 (1992)
107. L. Shao, N. Wex, Class. Quantum Gravity **29**, 215018 (2012)
108. T. Damour, G. Schäfer, Phys. Rev. Lett. **66**, 2549–2552 (1991)
109. P.J. Callanan, P.M. Garnavich, D. Koester, Mon. Not. R. Astron. Soc. **298**, 207–211 (1998)
110. K. Lazaridis, N. Wex, A. Jessner et al., Mon. Not. R. Astron. Soc. **400**, 805–814 (2009)
111. D.C. Backer, S.R. Kulkarni, C. Heiles et al., Nature **300**, 615–618 (1982)
112. L. Shao, R.N. Caballero, M. Kramer et al., Class. Quantum Gravity **30**, 165019 (2013)
113. S. Weinreb, J. Bardin, H. Mani, G. Jones, Rev. Sci. Instrum. **80**, 044702 (2009)
114. L. Blanchet, G. Schäfer, Mon. Not. R. Astron. Soc. **239**, 845–867 (1989)
115. L. Blanchet, G. Schäfer, Mon. Not. R. Astron. Soc. **242**, 704 (1990)
116. R. Nan, D. Li, C. Jin et al., Int. J. Mod. Phys. D **20**, 989–1024 (2011)
117. A.R. Taylor, Proc. Int. Astron. Union **8**, 337–341 (2012)
118. R. Smits, M. Kramer, B. Stappers et al., Astron. Astrophys. **493**, 1161–1170 (2009)
119. R. Smits, S.J. Tingay, N. Wex et al., Astron. Astrophys. **528**, A108 (2011)
120. M.A.C. Perryman, K.S. de Boer, G. Gilmore et al., Astron. Astrophys. **369**, 339–363 (2001)
121. S.M. Ransom, J.M. Cordes, S.S. Eikenberry, Astrophys. J. **589**, 911–920 (2003)
122. B. Allen, B. Knispel, J.M. Cordes et al., Astrophys. J. **773**, 91 (2013)
123. N. Wex, S.M. Kopeikin, Astrophys. J. **514**, 388–401 (1999)
124. K. Liu, Ph.D. thesis, University of Manchester, UK (2012)
125. N. Wex, K. Liu, R.P. Eatough et al., Proc. Int. Astron. Union **8**, 171–176 (2012)
126. K. Liu, N. Wex, M. Kramer et al., Astrophys. J. **747**, 1 (2012)
127. R.P. Eatough, H. Falcke, R. Karuppusamy, et al., Nature (2013), in press arXiv:1308.3147
128. G. Hobbs, A. Archibald, Z. Arzoumanian et al., Class. Quantum Gravity **27**, 084013 (2010)
129. B. Bertotti, B.J. Carr, M.J. Rees, Mon. Not. R. Astron. Soc. **203**, 945–954 (1983)
130. S.M. Kopeikin, Phys. Rev. D **56**, 4455–4469 (1997)
131. F.B. Estabrook, H.D. Wahlquist, Gen. Relativ. Gravit. **6**, 439–447 (1975)
132. S. Detweiler, Astrophys. J. **234**, 1100–1104 (1979)
133. A. Sesana, A. Vecchio, C.N. Colacino, Mon. Not. R. Astron. Soc. **390**, 192–209 (2008)
134. A. Sesana, A. Vecchio, M. Volonteri, Mon. Not. R. Astron. Soc. **394**, 2255–2265 (2009)
135. K.J. Lee, F.A. Jenet, R.H. Price, Astrophys. J. **685**, 1304–1319 (2008)
136. K.J. Lee, F.A. Jenet, R.H. Price et al., Astrophys. J. **722**, 1589–1597 (2010)
137. F.A. Jenet, A. Lommen, S.L. Larson, L. Wen, Astrophys. J. **606**, 799–803 (2004)